5-16-2017

Current understanding and future research directions at the onset of the next century of sintering science and technology

Rajendra K. Bordia
Clemson University, rbordia@clemson.edu

Suk-Joong L. Kang
Korea Institute of Ceramic Engineering and Technology

Eugene A. Olevsky
San Diego State University

Received: 22 February 2017 | Accepted: 6 March 2017

DOI: 10.1111/jace.14919

FEATURE ARTICLE

Journal of the American Ceramic Society

Current understanding and future research directions at the onset of the next century of sintering science and technology

Rajendra K. Bordia[1] | **Suk-Joong L. Kang**[2,3] | **Eugene A. Olevsky**[4]

[1]Department of Materials Science and Engineering, Clemson University, Clemson, South Carolina

[2]Korea Institute of Ceramic Engineering and Technology (KICET), Jinju, Korea

[3]Department of Materials Science and Engineering, Korea Advanced Institute of Science and Technology (KAIST), Daejeon, Korea

[4]Departmentof Mechanical Engineering, San Diego State University, San Diego, California

Correspondence
Rajendra K. Bordia, Department of Materials Science and Engineering, Clemson University, Clemson, SC
Email: rbordia@clemson.edu

Funding information
US National Science Foundation Division of Civil and Mechanical Systems and Manufacturing Innovations; NSF, Grant/Award Number: CMMI 1502392, CMMI 1234114

Abstract

Sintering and accompanying microstructural evolution is inarguably the most important step in the processing of ceramics and hard metals. In this process, an ensemble of particles is converted into a coherent object of controlled density and microstructure at an elevated temperature (but below the melting point) due to the thermodynamic tendency of the particle system to decrease its total surface and interfacial energy. Building on a long development history as a major technological process, sintering remains among the most viable methods of fabricating novel ceramics, including high surface area structures, nanopowder-based systems, and tailored structural and functional materials. Developing new and perfecting existing sintering techniques is crucial to meet ever-growing demand for a broad range of technologically significant systems including, for example, fuel and solar cell components, electronic packages and elements for computers and wireless devices, ceramic and metal-based bioimplants, thermoelectric materials, materials for thermal management, and materials for extreme environments. In this study, the current state of the science and technology of sintering is presented. This study is, however, not a comprehensive review of this extremely broad field. Furthermore, it only focuses on the sintering of ceramics. The fundamentals of sintering, including the thermodynamics and kinetics for solid-state- and liquid-phase-sintered systems are described. This study summarizes that the sintering of amorphous ceramics (glasses) is well understood and there is excellent agreement between theory and experiments. For crystalline materials, attention is drawn to the effect of the grain boundary and interface structure on sintering and microstructural evolution, areas that are expected to be significant for future studies. Considerable emphasis is placed on the topics of current research, including the sintering of composites, multilayered systems, microstructure-based models, multiscale models, sintering under external stresses, and innovative and novel sintering approaches, such as field-assisted sintering. This study includes the status of these subfields, the outstanding challenges and opportunities, and the outlook of progress in sintering research. Throughout the manuscript, we highlight the important lessons learned from sintering fundamentals and their implementation in practice.

KEYWORDS

composites, field-assisted sintering, grain growth, microstructure evolution, multilayered systems, multiscale models, review, sintering, sintering fundamentals, stress-assisted sintering

1 | INTRODUCTION AND OVERVIEW

Sintering has been practiced for thousands of years in the production of pottery. It has been nearly 100 years since the first published research on the sintering of ceramic materials in a scientific article by Ferguson* in 1918 in the first volume of the Journal of the American Ceramic Society.[1]

Since this publication, sintering has emerged as an important scientific and technological area. Illustrative of its importance, as of January 2017, Web of Science™ provides references to more than 108 000 publications on sintering-related topics. Despite this long history of research and development, sintering remains of tremendous relevance and importance as the most viable way to fabricate many novel materials, such as high surface area structures, nanopowder-based systems, and tailored functional materials. Testifying to the current significance of this topic to a broad spectrum of ceramics, there has been a focused meeting on sintering every 3 years with associate publications in the *Journal of the American Ceramic Society* and *Ceramic Transactions*.[2-6]

Sintering is the surface-tension-driven extension of the contact area between powder particles and grains by the transport of material to or around pores under appropriate conditions of temperature, pressure, and environment.[7] The overall goal of the sintering practice is to produce a coherent body (from rather fragile green bodies) with controlled microstructure—porosity and grain size. The emphasis of sintering and microstructural evolution theory, modeling, and analysis is to predict the path of the microstructural development and its dependence on controllable parameters (eg, temperature, time, environment, particle size, density, applied stress). Sintering and microstructural evolution have been the focus of sustained efforts to understand the thermodynamics and to develop models to quantify the kinetics. These efforts have been concurrent with many experimental studies to evaluate the theories and the effects of important process parameters. Readers are referred to many excellent reviews, monographs, and textbooks for in-depth information.[2-6,8-17]

In this Feature Article on the 100th anniversary of the first scientific paper in the *Journal of the American Ceramic Society* on the science of sintering, we provide an overview of the current understanding of this complex and important topic followed by a more in-depth look at contemporary and notable subtopics. Section 2 summarizes the fundamentals of sintering and microstructure evolution for crystalline materials sintered by the solid-state and liquid-phase mechanisms, and sintering of amorphous materials by viscous mechanism. Section 3 focuses on a continuum-mechanics-based macroscopic formulation of sintering, enabling the investigation of real-world practical problems of sintering of complex systems, including constrained sintering, sintering of composites, and sintering under applied stresses. This approach has been used to investigate important effects including shape evolution, spatial variation of relative density, and defect formation. Section 4 is focused on innovative and novel sintering approaches. In Section 5, the outstanding challenges and opportunities, as well as the outlook of progress in these areas are highlighted and in Section 6, some of the important aspects of sintering practice are presented. We also present three illustrative examples of how an understanding of sintering has been used to fabricate technologically important devices and systems.

2 | FUNDAMENTALS OF SINTERING AND MICROSTRUCTURE EVOLUTION

Sintering can be categorized into three types, solid-state sintering of crystalline materials (SSS), solid-state sintering of amorphous materials (or "viscous sintering"), and liquid phase sintering of crystalline materials (LPS). Irrespective of the sintering type, the final outcome is the bonding of particles and densification of powder compacts. For SSS and LPS growth (coarsening) of grains (particles) also occurs. Although insignificant at the beginning of sintering, especially in SSS, grain growth becomes substantial with densification and has a considerable influence on the final density and the resulting microstructure. Densification in amorphous materials occurs by the viscous flow of materials without any boundary between the particles.

*Ferguson, John Bright (1889-1963), the author of over 100 scientific papers, was an associate professor of physical chemistry at the University of Toronto (1920-48); he also spent 7 years with the Geophysical Laboratory in the Carnegie Institute of Washington, DC (presently Carnegie Institution for Science), where his historical paper on sintering of magnesia was written [see J.H. Marsh, The Canadian Encyclopedia, 2nd Ed., v. IV, p.829].

Sintering has commonly been divided into three overlapping stages—initial, intermediate, and final—based on the connectivity of the solid and the porous phase.[15,16] The initial stage is characterized by the bonding between adjacent particles with the formation and significant growth of necks but limited densification. Both the solid and the porous phase are connected. The intermediate stage involves considerable densification of the powder compact and in this stage the solid and the porous phase are connected. During the final stage, the solid phase is connected but the pores are isolated. For crystalline materials, in this stage, there is significant grain growth, and the microstructure evolution is controlled by the interaction between pores and grain boundaries.

During sintering of crystalline powder compacts, both in SSS and LPS, transport of the materials takes place from an atom source(s) to an atom sink(s) via detachment (an interface reaction) of atoms from the source, movement of atoms toward the sink (mostly by diffusion), and the attachment (an interface reaction) of atoms at the sink. Similar serial processes occur for grain growth from the surface of a small grain to the surface of a large grain across the grain boundary (for SSS) or through a liquid phase (for LPS). Therefore, the kinetics of bonding, densification, and grain coarsening, must be governed by the slower process, either diffusion or an interface reaction, a characteristic of serial processes. Conventionally, however, densification and grain growth in crystalline materials have been analyzed and predicted under the assumption that diffusion governs their kinetics.[15] This assumption has recently been found to be valid only for crystalline systems with rough (atomically disordered) interfaces.

In this section, for SSS and LPS, we first briefly review the classical understanding and description, based on the assumption of diffusion control. We then describe new perspectives on sintering and some related issues. We also provide a summary of the sintering of amorphous materials, a topic that is well understood. Additional topics of contemporary focus and future directions are presented in Section 4.

2.1 | Solid-state sintering (SSS)

Scientific models and descriptions of solid-state sintering started to be introduced from the middle of the 20th century. Frenkel[18] and, a year later, Pines[19] described the sintering process as viscous flow of matter and "evaporation of emptiness (vacancy)", respectively, leading to a reduction of the free surface energy. These two concepts, material flow and vacancy flow, have been the basis of all subsequent models and theories. From the 1950's to the 1990's, several kinetic models for the different stages of sintering were developed and have been discussed in the literature (including in books such as Refs. [15] and [16]). Here, we cite a few important publications. A critical assessment of initial-stage models is provided in Ref. [20]. The most widely accepted models for intermediate-stage sintering are presented in Refs [21–23]. The final-stage model is presented in Ref. [22] and is critically evaluated in Refs. [24] and [25].

2.1.1 | Classical description of bonding and densification

The driving force for material transport is the difference in the chemical potential of the atoms under curved surfaces.[15,16] For an idealized geometry of a powder compact as in Figure 1, due to this chemical potential difference, atoms are transported to the particle neck (the atom sink in bonding and densification) from the grain boundary as well as the particle surface (atom sources). The material transport from the particle surface to the neck surface entails redistribution of material on the surface of particles (bonding) without densification. The material transport from the grain boundary, on the other hand, induces densification (shrinkage of compact) as well as bonding. In the case of diffusion, the rate of material transport from the material source (grain boundary or particle surface) to the sink (neck surface) can be expressed as[15]:

$$\frac{dV}{dt} = JAV_m = \left(-\frac{D}{RT}\nabla\sigma\right)AV_m \quad (1)$$

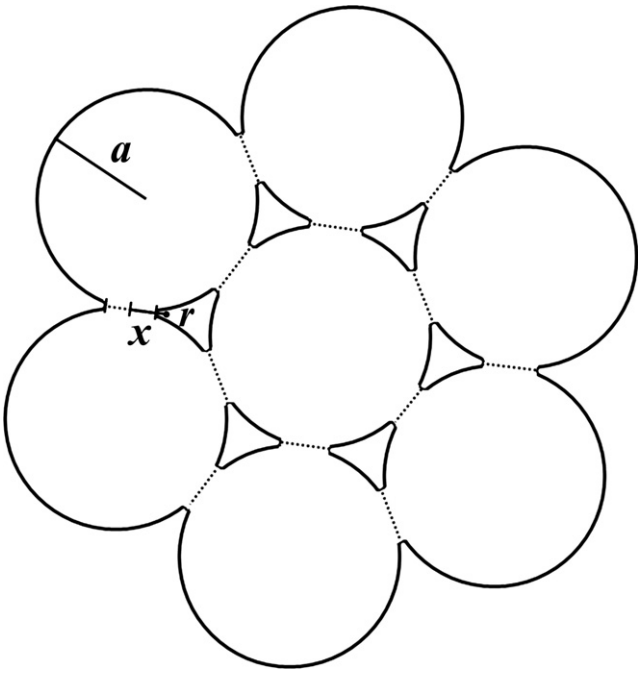

FIGURE 1 An idealized geometry of a powder compact on sintering. *a*: The radius of the particle; *x*: the radius of the neck between two particles; *r*: the radius of curvature of the neck

Here, V is the volume of material transported to the neck, t the sintering time, J the material flux, A the diffusional area, V_m the molar volume, D the diffusion coefficient, R the gas constant, T the absolute temperature, and $\nabla\sigma$ the stress (pressure) gradient.

For the initial stage (in general, for $x/a<\sim0.2$, where x is the radius of the neck and a is the radius of the particle) of bonding and neck growth, we can easily derive the kinetic equations, utilizing Equation (1). The kinetic equations take the following general form[15]:

$$\left(\frac{x}{a}\right)^n = F(T)\cdot\left(\frac{1}{a^{n-m}}\right)t \tag{2}$$

Here, $F(T)$ is a function of temperature, which includes a diffusion coefficient and absolute temperature, and n and m are exponents, which depend on the transport mechanism and the source of atoms.[15]

The microstructures of the intermediate and final stages of sintering are simplified and represented as channel-shaped interconnected pores along the grain edges and isolated pores at the grain corners, respectively.[22] The mechanisms that contribute to densification in these stages are grain-boundary diffusion and lattice diffusion from the grain boundary to the pore surface.[22-25] Using Equation (1), we can derive the kinetic equations for the intermediate and final stages. The general equation takes the form[15]:

$$\frac{1\mathrm{d}\rho}{\rho\mathrm{d}t} = \frac{K_1(1-\rho)^k}{G^m\rho} \tag{3}$$

Here, ρ is the relative density, K_1 is a constant containing various parameters, such as the diffusion coefficient, surface energy, temperature, and molar volume, k and m are exponents, which depend on the transport path, and G is the grain size. As the basic equation (Equation (1)), which was used to derive Equations (2) and (3), is the same, the qualitative dependences of neck growth and densification on sintering parameters are also the same.

As all the sintering mechanisms are operative at the same time, the contribution of each mechanism is additive and the dominant mechanism can be different for the same system under different experimental conditions. The result of all the contributions to sintering together with the sintering conditions for the dominant mechanism can be represented graphically using Ashby's "sintering diagram."[25-27] The major variables in conventional sintering (without external pressure) are particle size and temperature. The effect of size (scale) is commonly referred to as "Herring's scaling law",[28] which is expressed as the time required to achieve the same change in microstructure for samples of the same system but with different particle sizes of scale under an identical sintering mechanism. From Equation (2), the scale exponent is (n-m). The effect of temperature is more pronounced than that of scale as the diffusion coefficient includes the absolute temperature in an exponential function.

2.1.2 | Classical description of grain growth and microstructure evolution during sintering

During the intermediate and particularly in the final stage of sintering of crystalline materials, there is a strong interaction between grain boundaries and pores. In their classical experiment on Cu wires, Alexander and Balluffi showed that only the pores attached to the grain boundaries shrank.[29] It has been shown that as curved boundaries move during grain growth, the pores either remain attached to the boundary or are left behind. In the case in which they remain attached, the velocity of the boundary could be limited by pore mobility (boundary mobility higher than pore mobility) or by the intrinsic mobility of the boundary (pore mobility higher than boundary mobility). By using standard expressions for pore and boundary mobility, regimes of grain size and pore size in which separation occurs were identified.[30,31] This analysis was further refined and it was shown that the pore velocity is a function of dihedral angle and the pore size should be below a critical size (which depends on the grain size and dihedral angle) to avoid pore breakaway.[32,33] An additional analysis was carried out to include the effect of pore number density and pore size distribution on densification and grain growth.[34] Later, the effective mobility of boundaries with different pore sizes and pore shapes was calculated.[35]As long as diffusion-controlled grain growth occurs without the separation of pores from the grain boundary, the general grain growth kinetics can be expressed as[15]:

$$\frac{1}{G}\frac{dG}{dt} = \frac{K_2}{G^n(1-p)^l} \tag{4}$$

where K_2 is a constant containing several parameters, including the diffusion coefficient, boundary energy, absolute temperature, and molar volume, l and n are exponents. However, Equation (4) is valid only for idealized systems with a uniform distribution of grains and isolated pores at grain boundaries, and with grain growth controlled by pore mobility. Some experimental observations support this theoretical analysis on the grain growth in porous systems.[36-38] When the pore mobility is higher than the boundary mobility, there is no impeding effect of pores, and the kinetics of grain growth is the same as that of a dense material. In this case, the well-known square law (or parabolic law), where the square of the average grain size is proportional to the annealing time, is valid for normal grain growth even in porous materials.

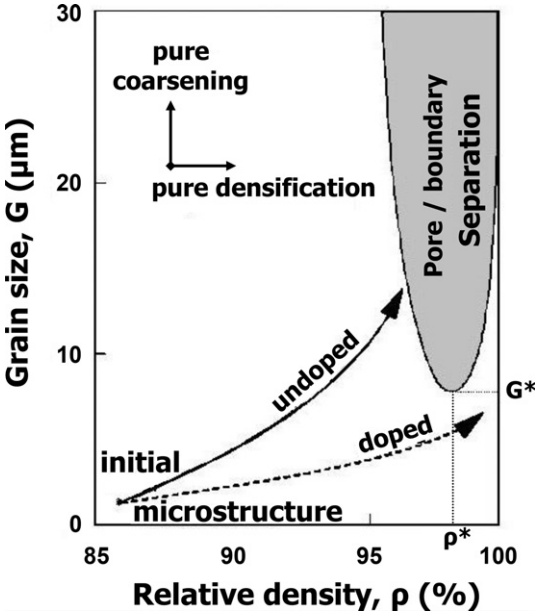

FIGURE 2 A schematic of the microstructural evolution diagram showing two different trajectories of undoped and doped samples (reprinted with permission from Elsevier)[15]

From Equations (3) and (4) a sintering trajectory dG/dρ can be obtained and represented as a microstructural evolution diagram on a grain size—density plane, as shown, for example, in Figure 2.[15] One relevant implication of the investigation of pore–boundary interaction has been the confirmation of the model experiment of Ref. [29] in many studies. For example, it has been shown that to prepare a fully dense material, pore/boundary separation must be avoided because the entrapped pores within grains cannot be eliminated, even by hot isostatic pressing.[39]

2.1.3 | Current issues in fundamentals of solid-state sintering

Since the middle of the 20th century, unconventional sintering techniques, which are different from the conventional pressureless sintering, have been developed to improve densification or suppress grain growth. The important unconventional techniques include pressure-assisted sintering, microwave sintering, two-step sintering, and electric field/current-assisted sintering. Except for pressure-assisted sintering, the mechanisms of densification enhancement or grain growth suppression of these unconventional sintering techniques are still a subject of debate or unclear. These techniques and the current status of the understanding of related sintering mechanisms are discussed in Section 4.

A current issue in the sintering community concerns the rate-limiting step of sintering kinetics. As mentioned earlier, all the models and analyses described in 2.1.1 and 2.1.2 are based on the assumption that the transport (diffusion) of atoms is the slower process and therefore rate controlling for the overall sintering kinetics. Recent investigations, however, show that the kinetics can be governed by the interface reaction of transported atoms rather than the diffusion of atoms when the boundary and the surface are atomically (even partially) ordered.[40,41] Figure 3 schematically depicts the microstructures of two samples being sintered for different boundary and surface structures, (A) rough (atomically disordered and macroscopically rounded) and (B) faceted (atomically ordered (smooth) and macroscopically straight or zig zagged).[42] For faceted boundaries and surfaces, experimental results, such as in Figure 4, show that densification can stop when the boundaries are well faceted.[40] (Compare the density plot with the change in grain-boundary structure, which is shown in the inset.) The results shown in Figure 4 indicate the presence of a critical driving force for densification in samples with faceted boundaries. It was also reported that the limiting density decreased with increased boundary faceting, which shows an increase in the critical driving force required for densification with an increasing degree of boundary faceting.[41] These results suggest that an interface reaction governs the densification of faceted systems when the driving force is smaller than a critical value.

The explanation of the correlation between the boundary faceting and the limit of densification relies on the assumption

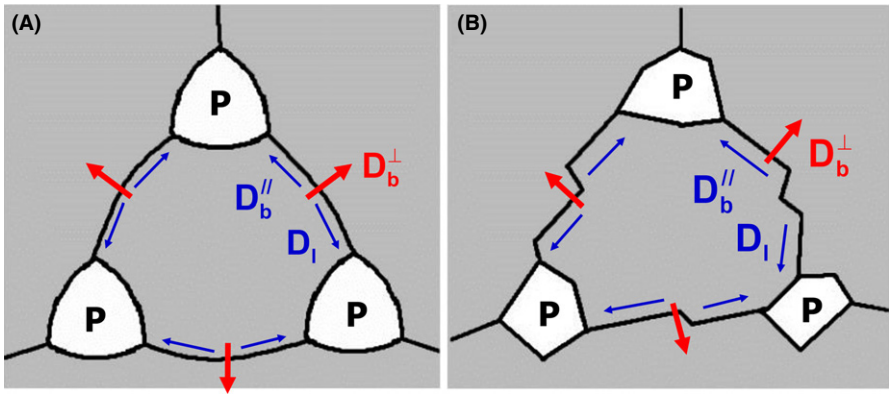

FIGURE 3 Schematic microstructures of two different samples being sintered with (A) rough and (B) faceted interfaces. P: pore; D_l: lattice diffusion; D_b'' and $D_b^{\perp}$: boundary diffusion along and perpendicular to the grain boundary. The red and blue arrows indicate, respectively, the direction of atom transport in grain growth and in densification.[42] (Reprinted with permission from Wiley-VCH Verlag)

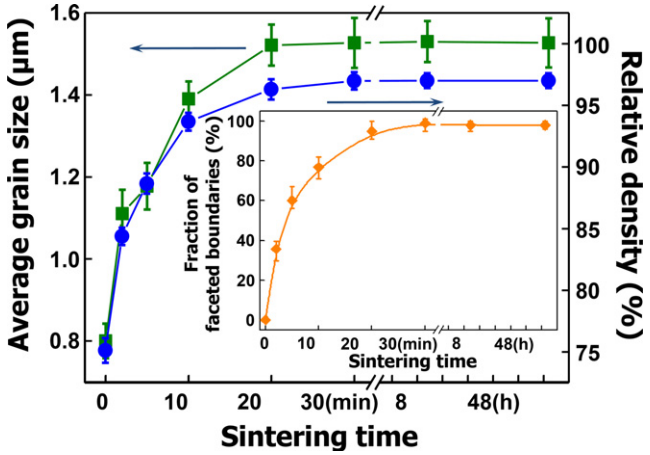

FIGURE 4 Densification (blue) and grain growth (green) of 0.4 mol%-TiO_2-excess $BaTiO_3$ during sintering in air after presintering in H_2 for 30 min. The inset is a plot of the measured fraction of faceted boundaries during sintering in air. Densification and grain growth stopped when the boundaries are well faceted (reprinted with permission from Elsevier)[40]

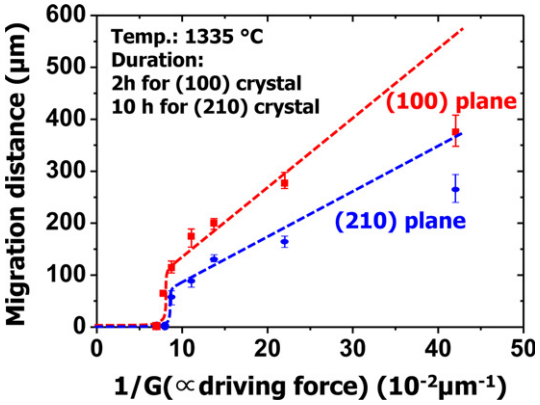

FIGURE 5 Measured migration distances of (100) and (210) planes of $BaTiO_3$ single crystals in $BaTiO_3$ polycrystals of different sizes during annealing of the single-crystal/polycrystal bi-layer samples. The driving force for the growth of a single-crystal seed remained constant during annealing as no grain growth occurred in the polycrystal (reprinted with permission from Elsevier).[52] A critical driving force is needed for appreciable migration of a faceted boundary

that the detachment of atoms from a faceted boundary controls the densification kinetics. A similar explanation, however, is also possible for the attachment of transported atoms at the faceted surface. At present, it remains unclear which process, detachment or attachment, governs the kinetics. The governing process may also be different from system to system. The above experimental results suggest a need for the development of a new sintering theory that takes into account the effect of the interface (boundary and surface) structure. It is also necessary to perform these types of experiments on other solid-state sintered systems in which the structure of the boundaries and surfaces can be systematically changed. If this mechanism is unveiled in other systems, then this may provide an explanation of why, in many systems, the diffusion coefficients measured from sintering do not match the diffusion coefficients measured from other experiments.

In the case of grain growth, the correlation between the boundary faceting and the boundary migration, as well as grain growth behavior, has been much more carefully studied.[43-51] As in the case of densification, Figure 4 indicates the presence of a critical driving force for grain growth in a sample with faceted boundaries. The migration behavior of faceted boundaries was also observed to be nonlinear with respect to the driving force for boundary migration (Figure 5).[52] Based on these experimental observations, Kang and co-workers suggested a mixed control mechanism of boundary migration, interface reaction control and diffusion control for a driving force smaller and larger than a critical driving force, respectively, and deduced the mixed mechanism principle of microstructural evolution.[53,54] The microstructural evolution principle is the result of the coupling between the critical driving force, Δg_c, for appreciable migration of the boundary and the maximum driving force, Δg_{max}, for the growth of the largest grain in the sample. Various types of grain growth behavior can appear in the same system with varying Δg_c and also Δg_{max}. An example of the application of the microstructural evolution principle can be found in the technical development of the solid-state conversion of single crystals.[55] Piezoelectric single crystals fabricated by the solid-state single-crystal growth method are now commercially available and are discussed in the Panel I.

Abnormal grain growth (AGG) has been an important area of intense investigation in the field of microstructure control. As described and discussed above, if there is a critical driving force for appreciable migration of grain boundaries in faceted systems (the rate controlling step changes with respect to the driving force for boundary migration), AGG can be well explained in terms of the coupling between Δg_c and Δg_{max}. Several other theories have been used to explain AGG focusing on the diffusion-controlled mechanism of grain growth, including the recently developed theory of grain-boundary phases called complexions,[58–63] solute drag,[64,65] and anisotropic grain-boundary energies and mobilities.[66–69] AGG in a few specific systems has been explained by both the nonlinear migration of faceted boundaries and the transition of boundary complexion with temperature.[70,71] Due to the breadth and the depth of this subfield, a thorough status report on this important topic is outside the scope of this study. In terms of sintering practice, one of the early success of the use of sintering fundamentals to develop commercially advanced ceramics was the development of approaches to suppress AGG resulting in translucent and transparent polycrystalline ceramics (Panel II).

PANEL I Solid-State Conversion of Single Crystals

Solid-state conversion of a single crystal from a polycrystal using a sintering process with microstructure control has been attempted for decades as a modern technique of single-crystal fabrication. The fabrication of single crystals in a solid state is feasible when grain growth, in particular AGG, in the polycrystal is suppressed while a seed crystal in or on the polycrystal grows and scavenges all the grains in the polycrystal. Figure A1 presents an example of solid-state conversion, showing the growth of a $Ba(Ti_{0.9}Zr_{0.1})O_3$ (BTZ) seed crystal into a sintered BTZ polycrystal.[56] Note that in the upper part of the polycrystal, an abnormal grain is formed and it will impede further growth of the single crystal grown from the seed in that direction. For grain growth control in a sintered polycrystal for solid-state conversion, the principle of microstructural evolution appears to be valid and useful.

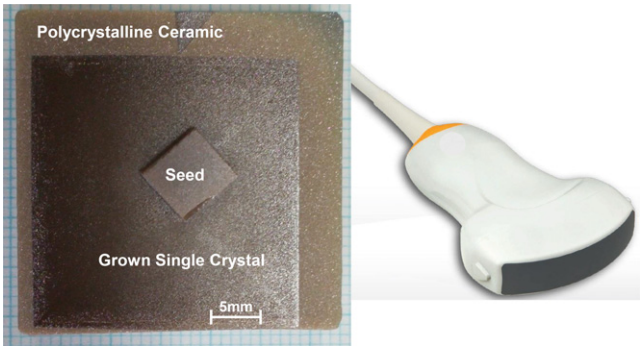

FIGURE A1 Microstructure showing the solid-state conversion of $Ba(Ti_{0.9}Zr_{0.1})O_3$. (Courtesy of Ceracomp Co., Ltd.) An ultrasound probe that contains piezoelectric single crystals is also shown. (Courtesy of Humanscan Co., Ltd.)

The solid-state single-crystal growth (SSCG) method offers notable advantages over the conventional melt growth and solution growth methods. The production cost is much lower than that of the melt growth method because of the much lower cost of equipment, with only simple furnaces being required for sintering and annealing. The uniformity and the versatility of the chemical composition of the produced single crystals are additional major advantages over the conventional methods. The net shape fabrication of single crystals is also possible by the SSCG method. Recently, the SSCG method was successfully adopted for commercial production of piezoelectric single crystals, including $(1-x)Pb(Mg_{1/3}Nb_{2/3})O_3$-$xPbTiO_3$ (PMN–PT) and $(1-x)Pb(Mg_{1/3}Nb_{2/3})O_3$-$xPb(Zr,Ti)O_3$ (PMN–PZT).[56]

The global market for piezoelectric materials is rapidly expanding, from US$ 6.5 billion in 2010 to 9.8 billion in 2014, along with an increased need for improved quality and functionality of sensors and actuators.[57] High-quality piezoelectrics, in particular single-crystalline materials and components, are even more in demand since the fourth industrial revolution focused on, for example, electronics, robots, connected devices, and smart cars. In accordance with this trend, the production of piezoelectric single crystals by solid-state conversion is expected to become significant in the future. Further development of this technique is also anticipated for fabricating single crystals for many other systems.

2.2 | Liquid phase sintering (LPS)

Liquid phase sintering (LPS) is commonly used for processing of a broad range of ceramics including porcelains, whitewares, insulators, abrasives, refractories, ferrite magnets, ferroelectric capacitors, cemented carbides (eg, Co-bonded WC), and covalent ceramics (eg, Si_3N_4).[75–77] In contrast to the conventional SSS of crystalline materials, in which densification occurs via the transport of atoms (an atomistic process), the densification in LPS can occur via a bulk (liquid) flow of material, similar to a viscous flow of amorphous material, as well as atomistic transport, similar to diffusional transport of atoms in solid-state sintering. In fact, two different densification models and theories, contact flattening with atom transport[78–81] and pore filling with a bulk material flow,[82–84] have been developed.

PANEL II Transparent Sintered Ceramics

Transparent crystalline ceramics offer distinct advantages compared to other transparent materials such as glasses and polymers. Specifically, they have better mechanical properties, chemical stability, high-temperature stability, and also transparency in the IR wavelengths. Many single-crystal oxides are transparent in visible and IR wavelengths. However, single crystals are expensive and difficult to fabricate in complex shapes.

For polycrystalline ceramics to be transparent, they must have very high density and clean boundaries as pores and second-phase particles on grain boundaries act as scattering sites. Furthermore, it is desirable to have a cubic crystal to minimize the scattering as light travels from one grain to another. The first successful attempts to make transparent polycrystalline ceramics were in late 1950s for sodium vapor lamps. GE introduced Lucalox@ sodium vapor lamps (Figure A2), which were made using MgO-doped alumina sintered in a hydrogen atmosphere at high temperature.[72] Since then, interest in transparent polycrystalline ceramics has continued to grow. Starting with high purity, chemically derived nanoscale powders a variety of processing techniques have been developed to make essentially full density ceramics while retaining fine grain size. Densification techniques include sintering (eg, transient second-phase sintering),[73] hot pressing, sintering to a closed pore state followed by hot isostatic pressing, and field-assisted sintering. These materials have excellent optical transmission and also good mechanical properties. Using these techniques, a wide variety of transparent ceramics have been developed including Al_2O_3 envelopes for sodium and metal halide lamps, doped yttrium aluminum garnet (eg, Nd-doped YAG) for high power lasers, various rare-earth garnets for scintillators,[74] Al_2O_3 for IR windows and domes (Figure A3), and Al_2O_3, AlON, and $MgAl_2O_4$ as transparent armor for ballistic applications.

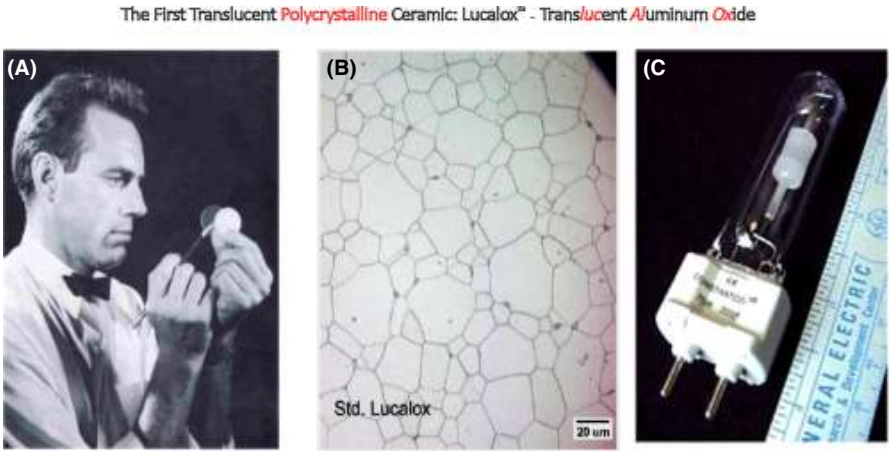

FIGURE A2 Robert Coble (A) invented Lucalox™ in September 1959 at the General Electric Research Lab. This dense, polycrystalline alumina (B) enabled the development of high-intensity discharge lamps (C). Images courtesy of GE [US Patent 3026210, 'Transparent alumina and method of preparation,' 1961]

FIGURE A3 CeraLumina™ alumina dome (Courtesy of CeraNova)

PANEL II Continued

Special thanks to Dr. Marina R. Pascucci, Director of Government Programs, CeraNova, Dr. A. Mark Thompson and Dr. Steven J. Duclos, GE Research, and Dr. William H. Rhodes, Rhodes Consulting for collaboration on preparing this Panel (transparent sintered ceramics) of the manuscript.

2.2.1 | Bonding and densification

The classical model of LPS[78–81] describes LPS as occurring via (i) rearrangement of particles with the formation of a liquid, (ii) material dissolution in and precipitation from a liquid, and (iii) atom transport through the liquid. The initial stage of particle rearrangement is a kind of bulk movement of grains and is due to an instantaneous capillary action of a formed liquid; its result is the distribution of liquid at the neck area between particles. This process leads to the bonding of particles with a liquid phase. In the earlier models, the contribution of rearrangement to densification was predicted to be significant,[16,80] but computer simulations have shown that this is not the case.[85] The second stage of dissolution/precipitation is characterized by material transport via atom diffusion through a liquid film from the contact area between particles to the off-contact area, resulting in flattening of the contact area. The contact flattening process is considered to be the major densification process and the appropriate kinetic equations have been developed.[78–81] These relationships including the dependence on important parameters such as the wettability of the liquid, liquid viscosity, and dissolution kinetics have been experimentally verified for a broad range of materials.[75–77,86–89]

One problem with the classical model for LPS is that this theory predicts a continuous reduction in the size of all the pores, causing a decrease in the relative population of large pores with increasing sintering time, as schematically shown in Figure 6A.[42] The grains in contact with pores are also expected to become more and more anhedral until the pores are completely eliminated (Figure 6A). Such predicted microstructural changes, however, have not been documented.

In a different model, the liquid filling of pores has been proposed as a fundamental process of LPS[82–84] based on microstructural observations in practical and model systems[90–92] and materials with a pore size distribution.[93] In this model, the liquid fills a pore by viscous flow driven by a difference in liquid pressure between the surface region of a pore that was being filled with liquid and the intact region of large pore surfaces.[94] As the wetting of the pore surface occurs as a result of an increase in the radius of the liquid menisci with grain growth, the pore filling occurs in temporal sequence, smaller pores earlier and larger pores later, and densification is induced by grain growth. The shrinkage of the sample after pore filling was explained as occurring via microstructural homogenization with preferential growth of grains into the liquid pockets formed at pore sites.[82,84] Although the physical mechanism of densification is the bulk flow of liquid, the time dependence of densification and shrinkage kinetics in the pore filling model is the same as that of the classical model because the densification is induced by grain growth, which occurs via atom transport through the liquid. The pore filling theory predicts the densification kinetics as functions of various processing and physical parameters, including the liquid volume fraction, pore volume fraction, grain size, wetting, and dihedral angle.[84]

One important microstructural characteristic in the pore filling theory is that the relative population of small pores decreases in the pore size distribution with increased sintering time or increasing grain size, as schematically shown in Figure 6B, which is different from the prediction of contact flattening (Figure 6A). In several LPS systems, especially those with a large volume fraction of liquid, this predicted evolution of the pore size distribution and the

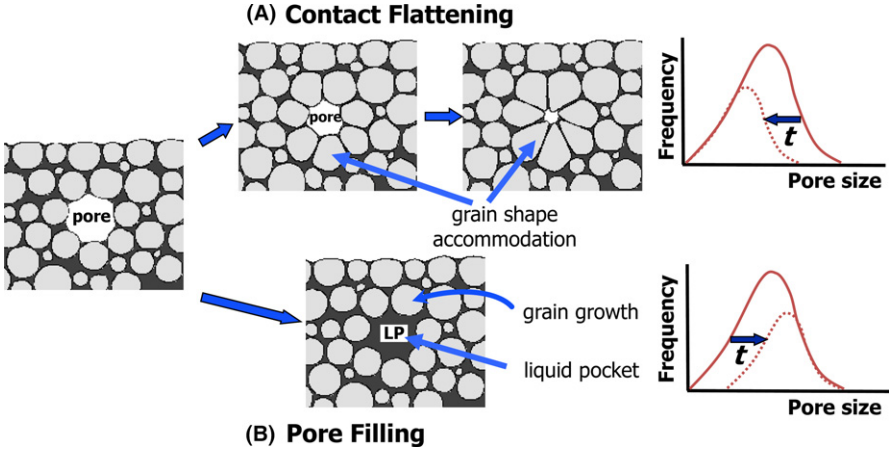

FIGURE 6 Schematic showing the expected changes in microstructure around a pore and pore size distribution during liquid phase sintering according to (A) the contact flattening and (B) the pore filling mechanism. The schematic grain size distribution shown with a dotted line is an expected distribution after sintering for a time t.[42] (Reprinted with permission from Wiley-VCH Verlag)

predictions of the densification kinetics from the pore filling model and theory have been confirmed.[92,95,96] A theoretical calculation showed that pore filling is the major densification mechanism in conventional LPS.[97]

2.2.2 | Grain growth and microstructure evolution during LPS

Grain growth in a liquid matrix, commonly referred to as Ostwald ripening, takes place with the shrinkage of small grains and the growth of large grains via dissolution/precipitation of atoms. The driving force for this process is the relative capillary energy of the grains. Ostwald ripening has long been studied theoretically, experimentally, and numerically since the 1960s with the development of the classical Lifshitz-Slyozov-Wagner (LSW) theory.[98,99] Although there have been modifications that took into account the effect of the volume fraction of liquid on grain growth kinetics,[100–102] the classical LSW theory has been the standard theory in interpreting experimental data of grain growth not only in solid–liquid two-phase systems but in two-phase solid-state systems (eg, precipitates in a matrix).

In the LSW theory, the interface mobility is assumed to be constant, irrespective of the driving force and the growth mechanism. As a result, the growth kinetics are proportional to the transport of atoms either through the matrix (diffusion) or across the interface (interface reaction). A cubic law is deduced for diffusion control and a square law for interface reaction control, which is similar to that for grain growth in single-phase systems. The interface reaction control of Wagner,[99] however, is physically a diffusion control across the interface because of the assumption of constant mobility. The relative grain size distribution predicted by the LSW theory is invariant (i.e., stationary) with respect to the annealing time, a consequence of a constant interface mobility and a characteristic of normal grain growth.

Adopting the pore filling theory for densification and incorporating it with grain growth kinetics, Lee and Kang developed the microstructural evolution diagram as a plot of density versus grain size, as in the case of SSS.[103] As the densification is induced by grain growth in the pore filling theory, the attainable density is governed by the average grain size, as presented, for example, in Figure 7. According to Figure 7, an increase in the liquid volume fraction results in a remarkable enhancement of densification, which is in agreement with experimental observations.

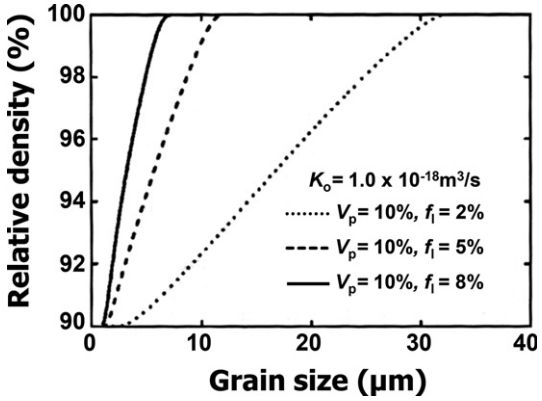

FIGURE 7 Calculated microstructural evolution diagram during liquid phase sintering showing the effect of liquid volume fraction according to the pore filling theory (reprinted with permission from Hanser Verlag).[103] K_o: grain growth constant; V_p: pore volume; f_l: liquid volume fraction

2.2.3 | Remarks on the fundamentals of LPS

The effect of the grain-boundary structure on the grain growth in liquid phase sintered systems is an area of intense investigation. Significant work has been conducted in recent years on the equilibrium structure and the state of grain boundaries, either with solute segregation or a liquid film, and their effect on microstructure evolution in ceramics and metals.[104–107] These studies have explored both normal and AGG. In this approach, AGG is due to the difference in the mobility of grain boundaries with different complexions in the same system.[58,69,107] This approach has explained the observed AGG in several systems with a limited volume fraction of liquid.[58,62,63,108]

Another approach to explain AGG observed in liquid phase sintered systems uses the growth behavior of a crystal with respect to its solid/liquid interface structure.[53,109–111] As in the case of the grain growth behavior in single-phase systems, the grain growth behavior in faceted, or even partially faceted, systems is not normal. The type of growth behavior was predicted and microstructural evolution was calculated in terms of the coupling of the critical driving force for appreciable growth of a grain and the maximum driving force for the growth of the largest grain in the sample (the mixed mechanism principle of microstructural evolution).[53,112] The AGG observed in many systems has supported this approach.[113–122]

As both of these approaches have been successful in explaining this important phenomenon in microstructure evolution, it is necessary to clarify the conditions for their applicability, although there has been discussion on them in a recent paper.[55] It is also important to establish whether the two approaches are contradictory or complementary.

2.3 | Sintering of amorphous materials—viscous sintering

For amorphous materials, sintering proceeds due to the transport of matter over the entire volume and, further, there are no grain boundaries and hence there are no coarsening

mechanisms and no grain growth.[15,16] For viscous sintering, the three stages have been analyzed by Frenkel (initial and final stage), Scherer (intermediate stage), and Mackenzie-Shuttleworth (final stage). The kinetics of viscous sintering can be calculated following the energy balance approach suggested by Frenkel.[18] Under quasiequilibrium, the energy gained by the reduction in surface area is dissipated due to viscous flow. Using this approach, Frenkel analyzed the kinetics of the initial stage of viscous sintering and developed the following relationship for the sintering of a pair of spheres by viscous flow[18]:

$$\theta^2 = \frac{3\gamma}{2\pi\eta a} t \tag{5}$$

where $\sin\theta$ is the ratio of the neck size to particle radius, γ the surface energy, η the viscosity, a the particle radius, and t the sintering time. Scherer[123] used a cell model to geometrically describe the intermediate sintering state and Mackenzie-Shuttleworth[124] following and advancing the original approach of Frenkel,[18] used the geometry of a spherical pore in a spherical shell as a model for the final stage. Both Scherer and Mackenzie-Shuttleworth used the energy balance principle proposed by Frenkel. It was shown that these two models predict the same densification rate over a broad range of the relative density (normalized by the theoretical density) of 0.3–1.[125] The densification rate from these models is given by:

$$\dot{\varepsilon}_f = -\frac{1}{2}\left(\frac{4\pi}{\eta}\right)^{1/3}\left(\frac{\gamma n^{1/3}}{\eta}\right)\left(\frac{1}{\rho}-1\right)^{2/3} \tag{6}$$

where n is the number of pores per unit volume, which can be calculated from the pore size and relative density, and ρ is the relative density. These models describe experimental results very well over a broad range of relative density, from sol-gel and silica-soot-derived low-density preforms to packing of glass particles.[126–128] These studies have also shown that in contrast to SSS and LPS, viscous sintering is insensitive to geometry, eg, particle size and shape, and particle and pore size distribution. As a result, relative density is the only state variable. Moreover, the material parameters such as viscosity and surface energy calculated from sintering studies match well with independent measurements of these parameters from other experiments.[126,128] As a result, for all practical purposes, sintering of amorphous ceramics (glasses) is well understood.

3 | CONTINUUM MECHANICS FORMULATION OF SINTERING

The sintering kinetics of real porous bodies is determined not only by the properties of the powder particles and the nature of their interaction but also by macroscopic factors. Among them are kinematic constraints (eg, adhesion of a porous sample to a furnace surface), externally applied forces, and inhomogeneity of properties in the volume under investigation (eg, inhomogeneity of the initial density distribution). In addition, materials or systems are often composed of different regions, which sinter at different rates (eg, composites or multilayered systems). In these cases, internal stresses are generated to maintain the strain compatibility. Technologically important examples include sintering of fiber optics cables,[129] complex multilayered electronic packages,[130] and composites. In other situations, sintering is conducted under external stresses (eg, hot pressing, sinter-forging). It is clear that these problems can be solved only in terms of a macroscopic description, which requires the response of a sintering body to a general state of stress. To address these challenges, continuum-mechanics-based approaches are necessary. Macroscopically, sintering under these complex conditions can be interpreted as a process of volume and shape deformation. To address these situations, the sintering body has been considered as a visco-plastic continuum and a mechanics-based approach has been developed and successfully applied, based upon the expansion of theories of plastic deformation of porous bodies. The basic concept of these analyses is the deformation of the body under a general state of stresses during sintering. Since the first introduction of the continuum-mechanics-based approach by Skorokhod,[131] this methodology has been further developed and periodically reviewed in comprehensive publications including, for example, a series of papers by Bordia and Scherer in the late 1980s,[132–134] the papers by Olevsky et al.,[135,136] and a review by Green et al.[137] The original rheological model of Skorokhod was refined to include a general state of stress[138,139] and the nonlinear response of the material.[135] In addition to being able to address complex sintering problems, this approach has been successfully implemented in finite-element analyses for optimizing the manufacturing of complex components.[135,140–148] An example of the type of problem that can be analyzed is shown in Figure 8, which presents the calculated density distribution in a sintered gear. The nonuniform sintered density distribution is because of nonuniform green density distribution due to pressing in a rigid die.

In this section, we provide the status of this approach including its use to investigate complex sintering situations such as the sintering of composites and constrained multilayer systems, and sintering under applied stresses.

3.1 | Isotropic constitutive laws

The general isotropic nonlinear constitutive relationship between the stress and strain tensor in the continuum theory of sintering[135] is represented below:

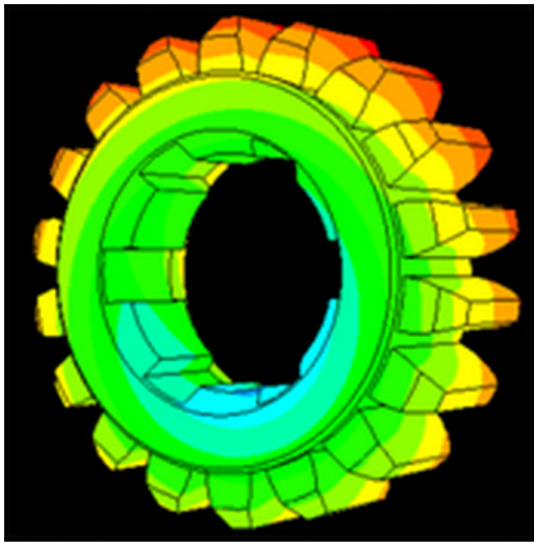

FIGURE 8 Finite-element simulation of free sintering of iron gear. Relative density distribution. The nonuniformity of density distribution is caused by pressing in a rigid die before sintering. The colors correspond to the spatial relative density distribution: green color corresponds to lower density levels and red color to higher density levels

$$\sigma_{ij} = \frac{\sigma(W)}{W}\left[\phi\dot{\varepsilon}_{ij} + \left(\psi - \frac{1}{3\phi}\right)\dot{e}\delta_{ij}\right] + P_L\delta_{ij} \qquad (7)$$

where ϕ and ψ are the normalized shear and bulk viscosities, which depend on the density and other microstructural parameters (such as grain size and relative interparticle neck radius), δ_{ij} is the Kronecker delta, and $\dot{e}$ is the first invariant of the strain rate tensor. Physically, $\dot{e}$ represents the rate of the volume change in a porous body. The effective equivalent strain rate W is related to the current porosity and the invariants of the strain rate tensor. The effective equivalent stress $\sigma(W)$ determines the constitutive behavior of a porous material. P_L is an effective sintering stress, which depends on the local sintering stress P_{Lo}, porosity and various pore structure parameters, such as relative interparticle neck radius. ("Effective" means that the parameter describes a value in a macroscopic porous volume, whereas "local" designates the parameters ascribed to a single pore or particle pair.) Various approaches have been developed to measure and calculate the sintering stress.[131,135,149,150]

An equivalent approach for linear viscous materials is to write the relationship between stresses and strain rates in the principal coordinate system using the free sintering rate, the uniaxial viscosity E_p, and the viscous Poisson's ratio v_p.[132,151] For isotropic sintering bodies, the constitutive relationship is as follows:

$$\dot{\varepsilon}_i = \dot{\varepsilon}_f + \left(\frac{1}{E^p}\right)\left[\sigma_i - \nu^p(\sigma_j + \sigma_k)\right] \qquad (8)$$

where *i, j,* and *k* are the three principal coordinate directions. Analog to linear elasticity, there are two relations between the four constitutive parameters, ϕ, ψ, E_p, and ν_p.[133] Thus, for an isotropic sintering body, only two constitutive parameters and the free sintering rate, $\dot{\varepsilon}_f$ (or the sintering stress, P_L), are required. For a sintering body, the viscous response to uniaxial stress (E_p), shear stress (ϕ), and hydrostatic stress (ψ), are function of both the powder compact's microstructure and density. Sintering microstructures are rather complex and includes several parameters, such as the relative density, average grain size, average pore size, grain size distribution, and pore size distribution. At the minimum, the respective models must be dependent on the relative density and should meet the limiting condition of incompressibility for the fully dense state. This corresponds to a viscous Poisson's ratio equal to 0.5 (equivalent to the bulk viscosity, $\psi \to \infty$).

For sintering of glass and particle filled glasses, this approach has been extremely successful. This is because, for these materials, the only state variable is the relative density (or porosity) and models have been developed for the constitutive parameters (E_p and ν_p) and the free sintering rate, $\dot{\varepsilon}_f$, in terms of the relative density. The free densification rate is given by Equation (6) presented in Section 2.3[123] and the viscous Poisson's ratio and the uniaxial viscosity are given by[151,152]:

$$\nu_p = \frac{1}{2}\left[\frac{\rho}{3-2\rho}\right]^{\frac{1}{2}} \qquad (9)$$

$$E_p = 2\eta\frac{\rho}{3-2\rho} \qquad (10)$$

For crystalline materials, the situation is more complex and both the free sintering rate and the models for the constitutive parameters depend on the sintering stage and additional microstructural parameters (eg, grain size and dihedral angle).[133,136,153–161] For example, Riedel et al.[158] proposed the following expressions for the shear and bulk viscosities in terms of the diffusion coefficients and material parameters for intermediate-stage sintering controlled by grain-boundary diffusion

$$\varphi = \rho_0\rho^{\frac{1}{3}}Z\frac{3c^2}{20a}\left\{\frac{kTc^4}{12\Omega\delta D_b} + \eta_s\right\} \qquad (11)$$

$$\psi = \frac{\rho_0^{2/3}\rho^{1/3}ZkTc^4}{48\Omega\delta D_b a} \qquad (12)$$

where ρ_0, Z, c, a, and η_s are, respectively, the initial relative density, the average number of contact per particle, the grain size, the particle radius, and the sliding viscosity between particles. Parameters *k, T,* δ, Ω, and D_b are, respectively, the Boltzman constant, absolute temperature,

grain-boundary thickness, atomic volume, and the grain-boundary diffusion coefficient.

A variety of techniques have been used to experimentally measure the constitutive parameters. The most common approach has been using a "loading dilatometer" or the "sinter-forging" unit.[161–165] In this approach, a constant axial stress (or load) is applied to a sintering body and the axial and radial strain rates are measured.[133,135,166] Knowing the stress and the two strain rates, and also carrying out the same experiments without applied stresses (free sintering), all the constitutive parameters can be measured. The parameters have been measured for a wide range of materials. It has been shown that the relative density based models are quite successful in predicting the measured constitutive parameters for glasses or glass matrix composites that sinter by viscous flow.[167] However, the measured constitutive parameters for polycrystalline ceramics (which sinter by solid-state diffusion) did not agree with the microstructure-based models. In a critical study, it was shown that this was due to the anisotropy that was induced in polycrystalline materials sintered under constant uniaxial stress.[168] Two modified approaches, discontinuous sinter-forging[169] and cyclic sinter-forging,[170] have been developed. Using these techniques, isotropic constitutive parameters, which match the microstructural models well, have been obtained.[169–172]

3.2 | Sintering of composites

There is considerable interest in sintering ceramic matrix composites. Starting in the 1980s, controlled experiments were conducted on both glass matrix and polycrystalline ceramic matrix composites.[162,173–180] From these and other studies, the following overall conclusions can be drawn:

1. There are two distinct cases: (i) the minority phase sinters at a rate slower than the matrix and (ii) the minority phase sinters faster than the matrix. Most studies have been conducted on the first case.
2. For a low volume fraction, below the percolation threshold, the overall densification rate is governed by the densification rate of the matrix. However, the slower densifying minority phase reduces the densification rate of the composite more than the rule of mixtures.
3. If both phases are connected, then the composite densification rate is controlled by the slower densifying phase.
4. Sintering of composites has the potential to introduce crack-like processing defects that can be strength-limiting flaws, as shown in Figure 9.[181]

Continuum models have been developed to calculate the densification rate of composites with a low volume fraction of a second phase.[135,153,182,183] The conditions for the formation of processing defects have also been analyzed.[153,182] The various models for densification of composites were reviewed in Ref. [134]. These models qualitatively predict the experimental observations including the effect of inclusions on the densification rate of the matrix and the conditions under which processing defects can form. For glass matrix composites, the quantitative prediction has been excellent.[176,178,179,184] The match between experiments and analysis has also been very good for matrices that sinter by liquid phase sintering.[185] However, this approach has not been successful in quantitatively predicting the densification rate of polycrystalline matrix composites.[134] Specifically, the observed reduction in the densification rate and the total density change is greater than predicted by the analysis.[134,162,180]

3.3 | Sintering of multilayered systems and constrained films

Ceramic multilayers are important in wide-ranging applications including, for example, electronic packages, multilayer capacitors, ceramic sensors and actuators, batteries, and solid oxide fuel cells.[186–189] Similarly, there are many applications of ceramic coatings including, for example, environmental and thermal barriers, wear resistance, corrosion prevention, and biocompatible coatings.[190] As a result, the sintering of multilayered ceramic systems and constrained films has been extensively studied.

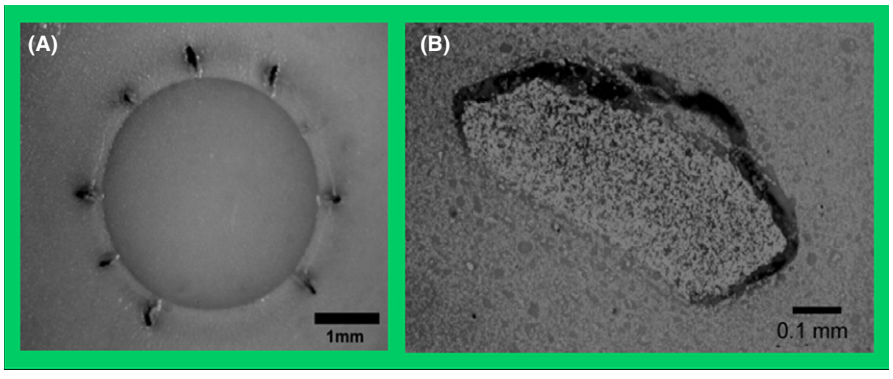

FIGURE 9 Cracks due to differential densification in composites. (A) Radial cracks around a rigid (fully dense) alumina inclusion in a sintering alumina matrix; (B) circumferential cracks around a faster sintering alumina agglomerate in an alumina matrix.[181] (Courtesy of Dr. S.M. Salamone)

The above-mentioned cases are specific examples of differential co-sintering (or co-firing) in which the common feature is that there are two or more porous materials with different inherent (free or unconstrained) densification behavior. The difference in the densification behavior is due to the two or more materials being chemically different or having different physical characteristics that control the densification behavior (eg, particle size, green density). The compatibility conditions require modification in the sintering behavior due to the presence of another material/system in physical contact. A typical situation is schematically shown in Figure 10.[191] Due to the constraint, the densification behavior of the two layers is modified. The densification rate of the slower densifying layer is enhanced and that of the faster densifying layer is retarded. In addition, there is the possibility of the formation of defects and shape distortions. Experimentally observed phenomena including warping, formation and growth of cracks, and delamination are shown schematically in Figure 10. Both experimentally and theoretically, it has been shown that the critical parameter in the processing of multilayered systems is the difference in the unconstrained densification rates between the two layers. A limiting extreme case is the sintering of porous materials on fully dense stiff substrates. This situation is called constrained sintering and has been the focus of many investigations. Ref. [191] provides a comprehensive review of this problem.

The densification behavior of a constrained film sintering on a substrate has been analyzed using the continuum approach.[192–194] Using isotropic constitutive laws, for a fully constrained film (eg, a thin film on a rigid substrate), it has been shown that the densification rate of the constrained film is given by[192]:

$$\left(\frac{\dot{\rho}}{\rho}\right)^{\text{constr}} = \frac{1+\nu^{p}}{1-\nu^{p}}\frac{1}{3}\left(\frac{\dot{\rho}}{\rho}\right)^{\text{free}} \tag{13}$$

where $\left(\frac{\dot{\rho}}{\rho}\right)^{\text{constr}}$ is the densification rate of the constrained film and $\left(\frac{\dot{\rho}}{\rho}\right)^{\text{free}}$ is the densification rate of the same film but without the constraint from the substrate and ν^{p} is the viscous Poisson's ratio.

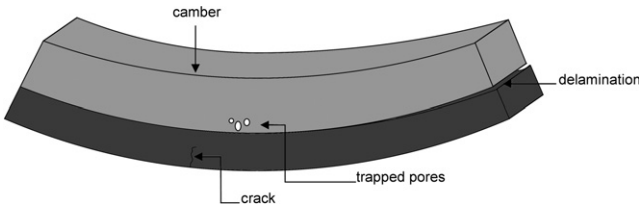

FIGURE 10 Schematic geometry of sintering of a bi-layer system illustrating the type of processing defects that may form and the expected shape distortion. The top layer has a faster sintering rate. (Courtesy of Dr. J. B. Ollangnier)

The densification behavior of constrained films has been experimentally investigated for a wide variety of glass and ceramic films including, for example, alumina,[195,196] titania,[197] zirconia,[198] zinc oxide,[136] glass,[192,199] and glass–ceramics.[200–202] It has been shown that the continuum approach using isotropic constitutive laws is able to quantitatively predict (or explain) the densification behavior of amorphous sintering systems (glass and glass–ceramics). As a result, the approach has been successfully implemented in detailed numerical codes for processing of multilayered systems that require extremely fine dimensional control such as multilayered electronic packages.[136,186,187] However, this approach overestimates the densification rate of solid-state sintered constrained films (polycrystalline ceramics). This is illustrated in Figure 11.[195] One possible reason for this discrepancy is the development of anisotropic microstructure during constrained sintering.[203] Discrete-element simulations have also shown that the microstructure becomes anisotropic during constrained sintering.[204,205]

Another significant problem in constrained sintering is that when a film is sintered on a nonsintering (or slower sintering) substrate, in-plane tensile stresses are generated in the film, which can result in the formation or growth of defects in the film during sintering. This phenomenon has been experimentally observed in both constrained sintering of glass and ceramic films.[206–208] This problem has also been analyzed using the continuum formulation and the conditions for crack growth have been established.[206] It has been concluded that constrained films are most susceptible to cracking during the early stage of sintering

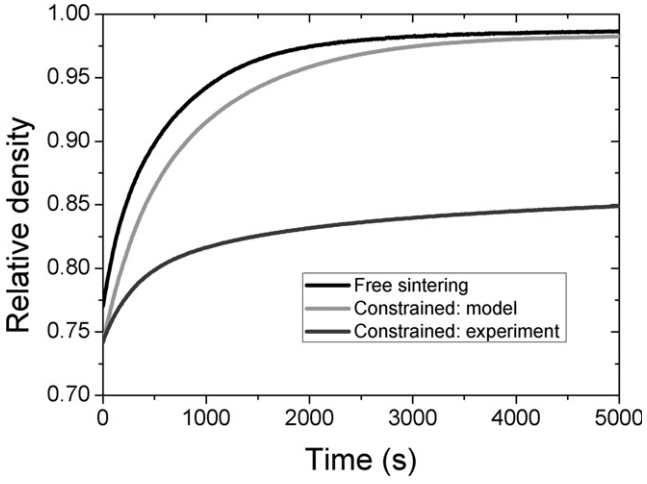

FIGURE 11 Constrained densification of crystalline films (alumina) on a rigid substrate compared to free sintering and predictions of constrained densification from isotropic continuum models. Dramatic reduction in the densification rate and final density of the constrained film. The isotropic model is not able to predict the densification of constrained films.[195] (Reprinted with permission from Wiley)

(highest densification rate which leads to the generation of defects and the lowest crack growth resistance due to small interparticle contacts). It has been shown that there is a critical film thickness (normalized by the particle size), which is influenced by the interfacial bonding between the film and the substrate. If the film thickness is less than the critical thickness, the cracks and defects in the constrained film do not grow. In addition, there is a critical crack/defect size (normalized by the particle size) such that cracks smaller than this size do not grow.[206] Experimentally, the existence of a critical film thickness has been confirmed for both glass and ceramics, but the critical crack size, which is of the order of 25 times the particle radius, has not been demonstrated.[206] Discrete-element simulation has shown that another important parameter is the interparticle sliding resistance. Cracks and defects are less likely to form in systems in which the interparticle sliding resistance is low.[209]

In part due to its technological importance, the sintering of multilayered systems has been a topic of significant focus. An important effect in multilayered systems, not generally observed in sintering of thin films on rigid substrates, is the warping of a multilayered assembly.[136,210] Several investigators have studied the evolution of the warping of bi-layer assemblies and the associated development of stresses using isotropic constitutive laws; they showed good agreement of the calculated warping with experimental results.[136,200,202,207,210–213] Huang and Pan[214] noted that obtaining the material constitutive properties is a cumbersome task. They proposed an empirical numerical method to calculate the sintering deformation without knowing the material parameters. The method, based only on the knowledge of the free sintering curve, is valid when no external force is applied and predicts the same distortion of a thin film on a rigid substrate as the full constitutive model.[214] Using a comprehensive theoretical analysis of densification and shape distortion of bi-layer and tri-layer systems, Olevsky and co-workers developed a framework in which all the necessary parameters for predicting the shape distortion of a bi-layer system can be obtained from the free densification behavior of the material of each layer and the densification behavior of a tri-layer symmetric system.[215,216]

3.4 | Sintering under high external uniaxial stresses

This manuscript is primarily focused on free sintering, which is a thermally activated transition of a powder (or a porous system) to a more thermodynamically stable state, through a decrease in the free surface energy. However, in many technologically important cases, ceramics are sintered under external stresses—hot-pressing, hot isostatic pressing, hot drawing, and sinter-forging. A comprehensive assessment of this vast field is beyond the scope of this manuscript. Here, we provide a brief overview of these techniques with a focus on the connection of these processes to other topics covered in detail here—continuum mechanics approach to sintering and spark-plasma sintering. The hot-forming processes can be classified into low or high stress processes based on the value of the external stress relative to the sintering pressure.

For hot deformation processes at high stresses, experimental results indicate that the dominant mechanism is the power-law creep,[217] which is usually described by:

$$\frac{\sigma}{\sigma_0} = A\left[\frac{\dot{\varepsilon}}{\dot{\varepsilon}_0}\right]^m \tag{14}$$

where σ and $\dot{\varepsilon}$ are the stress and strain rate, respectively; A, σ_0, $\dot{\varepsilon}_0$, and m are material parameters.

The nonlinearity of the governing relationship (Equation 14) between stresses and strain rates in hot deformation processes is reflected in the respective expressions of the constitutive parameters of porous bodies subjected to high-temperature, high-stress deformation. Several models have been proposed for the constitutive parameters.[135,218–225] For example, Helle et al. used a micromechanical approach to find the effective resistance of the powder body to externally applied loads under conditions of hot isostatic pressing.[218] Besson and Abouaf utilized experimental studies to derive the values of bulk and shear viscous moduli of a hot-pressed powder material.[220] Sofronis and McMeeking utilized finite-element methods and proposed a model for the collapse of isolated pores in a nonlinear viscous medium.[221] Geindreau et al. also used a nonlinear framework but employed a semi-experimental approach.[223] Castaneda and Willis used variational principles to obtain a nondilute (self-consistent approximation) and strain rate sensitivity-dependent expression of the bulk viscous modulus.[219]

Using the continuum theory of sintering, Olevsky and Molinari derived a nonlinear formulation for the pressure-assisted sintering techniques in a generalized form[224]:

$$\sigma_z = \frac{\sigma(W)}{W}\psi\dot{e}\left[\sqrt{\frac{2}{3}}\mathrm{sgn}(\sigma_z(n)+1\right] \tag{15}$$

For this case, similar to Equation (14),

$$\frac{\sigma(W)}{\sigma_0} = A\left(\frac{W}{\dot{\varepsilon}_0}\right)^m$$

The parameter n in Equation (15) assumes the following values for different loading modes: n=0 for isostatic pressing; $n\longrightarrow\infty$ for pure shear; $n=-\sqrt{6}$ for forging; and $n=\sqrt{6}$ for drawing. For the case of pressing in a rigid die, n becomes dependent on the porosity: $=\sqrt{\frac{2}{3}}\mathrm{sgn}(\dot{\varepsilon}_z)\frac{\phi}{\psi}$, which causes additional complexity.

It should be noted that these modeling concepts of powder hot-pressing have recently been utilized for the analysis of spark-plasma sintering (SPS) processes.[225,226] For SPS, these numerical codes use the constitutive parameters to describe the pressure-assisted deformation of the powder compact and use the temperature of the process from Joule heating due to the passage of the electric current. In this sense, they lack the distinguishing specifics of field-assisted processing (see Section 4.1).

3.5 | Current issues in continuum formulation of sintering—anisotropic microstructure

We next focus on one special case of sintering under a small uniaxial stress (of the order of sintering pressure) in an open die, also called sinter-forging, to highlight one of the current focal areas in the subfield of continuum formulation of sintering.

The original rheological framework for sintering bodies was developed to understand the densification and deformation behavior under external stresses.[131,133,135,151] During sinter-forging, the powder compact is subjected to a rather simple and uniform stress state—a uniaxial compressive stress (assuming low friction between the sample and the loading platens). This thus represents a good test case for the assessment of the continuum formulation of sintering. Therefore, as summarized in Section 3.1, sinter-forging in loading dilatometers has been commonly used to obtain the constitutive parameters for sintering bodies. For glasses it has been shown that, knowing the constitutive parameters, the densification and deformation under uniaxial stresses can be accurately predicted.[151,227,228]

However, this has not been the case for solid-state sintered crystalline materials. A good critical test of the analysis is the "zero radial strain rate sinter-forging experiment". In this experiment, an axial compressive stress is applied on a sintering body and the stress is adjusted to ensure that the radial strain rate is equal to zero at all times. Using the isotropic continuum formulation, this stress is calculated to be:

$$\sigma_z = \frac{E_p \dot{\varepsilon}_f}{\nu_p} \tag{16}$$

Thus, knowing the free densification rate, the uniaxial viscosity, and the viscous Poisson's ratio, the required stresses for zero-radial strain rate can be calculated. The calculated and measured stress for alumina is plotted in Figure 12, which clearly shows that the calculation underestimates the necessary stress for all densities.[229] One possible explanation is that it has been observed that during sinter-forging, the microstructure becomes anisotropic.[168,230] Figure 13 shows anisotropic pore orientation for sinter-forged samples. Therefore, it has been argued that

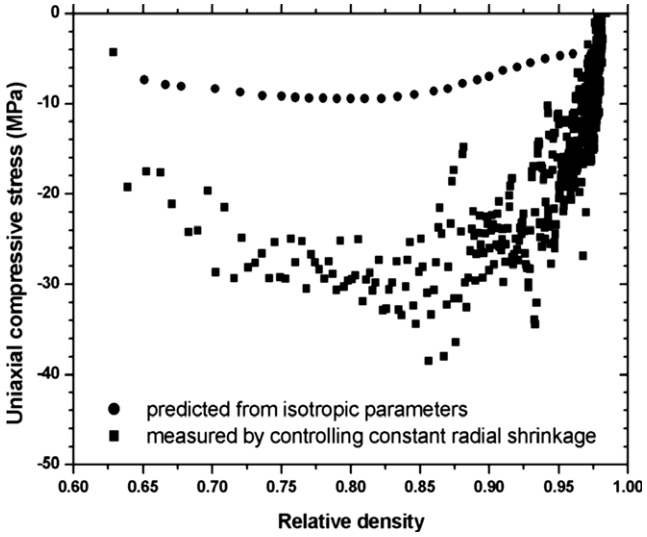

FIGURE 12 Calculated, using isotropic continuum models, and measured uniaxial stress needed for zero-radial shrinkage during sinter-forging as a function of density. The calculated stress is significantly lower than the experimental stress required.[229] (Reprinted with permission from Elsevier)

using isotropic constitutive parameters and the related formulation is not appropriate.[229] Discrete-element simulation also showed that due to sinter-forging, the microstructure becomes anisotropic.[231]

Both the sinter-forging and the constrained sintering problems have a transversely isotropic symmetry. To investigate these problems, a transversely isotropic continuum formulation has been developed. For a transversely isotropic (isotropic in 1-2 plane) body undergoing linear viscous deformation with densification, the constitutive relations in terms of the stress and strain in the principal coordinate system can be written as[135,229] (compared with Equation (8) for isotropic symmetry):

$$\dot{\varepsilon}_1 = \dot{\varepsilon}_2 = \dot{\varepsilon}_3^{\text{free}} + \frac{1}{E_1^P}\left[\sigma_1 - \nu_{12}^p \sigma_2 - \frac{E_1^P}{E_3^p}\nu_{31}^p \sigma_3\right] \tag{17}$$

$$\dot{\varepsilon}_3 = \dot{\varepsilon}_3^{\text{free}} + \frac{1}{E_3^p}\left(\sigma_3 - \nu_{13}^p \frac{E_3^p}{E_1^p}(\sigma_1 + \sigma_2)\right) \tag{18}$$

Equations (15) and (16) are based on the two sets of constitutive parameters that control the anisotropic sintering phenomena. These two sets can be identified as parameters associated with the anisotropic deformability of the porous material (viscosity and viscous Poisson's ratio) and parameters associated with anisotropic driving forces (sintering stresses or free sintering rate). Instead of the three constitutive parameters for the case of an isotropic body, six constitutive parameters are now required. Experimentally this will be quite challenging and thus, there is a need to determine these parameters using multiscale

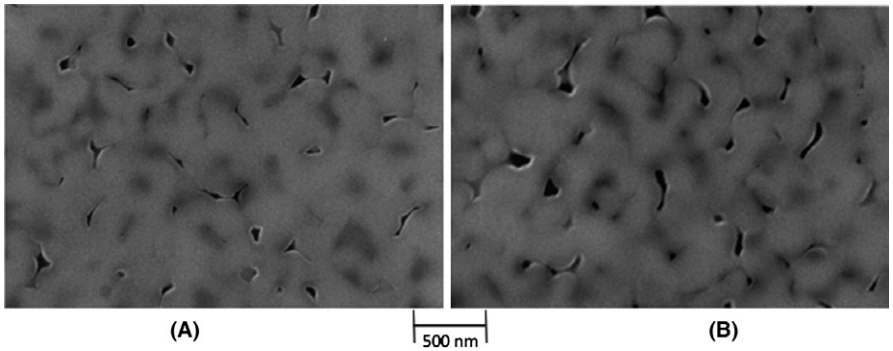

FIGURE 13 Microstructural images of alumina samples with a final density of 80% attained by (A) free sintering and (B) sinter-forging, respectively, at 1250°C. The applied uniaxial stress is approximately 2 MPa along the "z" direction (vertical in the figure). Clear evidence of anisotropic microstructure in sinter-forged samples.[168] (Reprinted with permission from Wiley)

modeling.[231–234] The multiscale modeling of sintering is discussed in Section 6.1.

In summary, we emphasize that the isotropic continuum formulation has been successful in modeling the densification and deformation of composites and constrained films, and the sintering under stresses for materials that sinter by the viscous sintering mechanism (glasses and composites with a significant volume fraction of glasses). This has had a significant technological impact on developing robust and reliable processing protocols for many important systems including, for example, multilayered electronic packages and multilayered ceramic capacitors (Panel III). However, we note that in the SSS systems, the microstructure has been shown to become anisotropic during constrained sintering or sinter-forging. For these systems, the isotropic formulation is not adequate to explain the experimental results. Thus, there is a need for the following:

1. Identification of state variables to describe the state of anisotropy in these systems.
2. Development of multiscale simulation protocols for calculation of the anisotropic constitutive parameters.
3. Identification of critical experiments to test the calculated constitutive parameters.
4. Careful experimental validation of the calculated anisotropic constitutive properties.
5. Use of these anisotropic constitutive laws to explain the experimentally observed constrained densification behavior of SSS films and composites, and their response to external stresses (eg, stress required for zero-radial rate sinter-forging experiment), which cannot be explained by the isotropic continuum formulation.

4 | INNOVATIVE AND NOVEL SINTERING TECHNIQUES

There is continuing demand to develop techniques that can effectively and predictably control the microstructure of powder-processed materials. Specifically, for crystalline materials due to the rapid grain growth in the final stage of sintering, the potential of traditional thermomechanical methods is limited in terms of fabricating materials with nanostructured microstructures. It has been shown that the densification of powders under external electromagnetic fields provides a finer control over the microstructure and enables the fabrication of nanostructured materials. This topic is the focus of this section with an overview of the various modern approaches that have been developed to enhance densification and suppress grain growth.

4.1 | Spark-plasma sintering (SPS) or Field-Assisted Sintering (FAST)

Spark-plasma sintering, also known as electric-discharge sintering and field-assisted sintering, was originally developed to process hard to densify materials and to control their microstructure.[237,238] A number of comprehensive review articles highlighted various aspects of SPS.[239–241] The technique is also gaining commercial importance as is evident from the large number of patents issued for this process.[242] A schematic of the process is shown in Figure 14.[243] SPS significantly shortens the processing of powder materials and improves the powder consolidation performance in terms of both time and quality. It has become especially useful for densifying hard to sinter ceramics including carbides, nitrides, borides, and composites. It is also promising with regard to maintaining the nano and submicrometer structure in nanopowder-based materials. With a current focus on nanostructured materials, SPS has become very popular as one of the few processing techniques to produce dense fine-grained samples from high-melting point ceramic powders.[238–240] SPS has also been found to be a versatile technique to join hard to join dissimilar materials.[238,244–246]

In this class of processes, the porous body is hot-pressed and a unique feature is that heating of the sample is accomplished by passing electric current through the die or through conductive samples. The difference between the known field-assisted sintering approaches is in the method and nature of electric current. For example, in the SPS

PANEL III Multilayer Ceramic Capacitors

The fabrication of multilayer ceramic capacitors (MLCCs) gives a typical example of the success of our understanding of constrained sintering of multilayered, multimaterial systems. A multilayer ceramic capacitor consists of alternating layers of dielectric material, mostly $BaTiO_3$ with additives, and an electrode, commonly Ni, as shown in Figure A4. With the development of electronic and electrical products with miniaturization and multifunctionalization, high-capacitance miniature MLCCs have been in increasing demand. As a result, technological developments in MLCC fabrication have been significant in the last two decades. The size of MLCCs has been reduced from 3.2 mm×1.6 mm to 0.2 mm×0.1 mm and MLCCs of a smaller size are expected to be produced.[235] The thickness of the dielectric layer has been reduced from a few micrometers to a level of a few tenths of a micrometer and the number of layers has reached 1000 for some products. In producing high-end MLCCs, a critical issue is uniform and predictable shrinkage of dielectric and electrode layers and control (suppression) of grain growth in the layers. Further theoretical as well as experimental studies on the sintering of nanosized $BaTiO_3$ particles and their MLCCs are required for continued development of MLCCs.

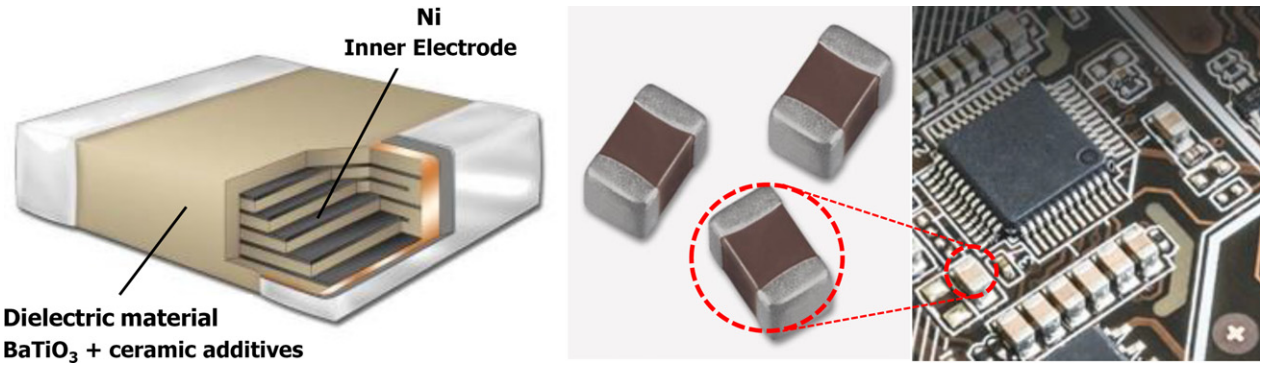

FIGURE A4 Schematic showing dielectric ($BaTiO_3$) and electrode (Ni) layers of MLCC. The two pictures are MLCC chips and many mounted MLCCs within an electronic device. (Courtesy of Samsung Electro-Mechanics Co. Ltd.)

MLCCs are widely utilized as an essential passive component in electronic devices and products for everyday use, such as mobile phones, televisions, computers, displays, and vehicles. Approximately 800 MLCCs are embedded in a high-end mobile phone and 2,000 in an LED television. The global market for MLCCs in 2015 was US$ 6.5 billion and is expected to reach US$ 7.5 billion in the year 2020. The use of MLCCs in the auto industry is rapidly increasing. About 3500 MLCCs are currently used in a current medium size car and more than 10 000 MLCCs are used for an electric vehicle. With the growth of the car industry, the MLCC market in this area is expected to increase by over 10% a year and to reach US$ 1.8 billion in the year 2020.[236]

process, a pulsed DC field is applied from the beginning to the end of the sintering cycle, whereas in Plasma Activated Sintering (PAS) a combination of pulsed and continuous DC current is used, and in Electroconsolidation an AC field is used. Electric current passage can provide a very fast heating rate (usually up to 600°C/min) during powder consolidation in comparison to the conventional radiation heating (2–30°C/min). The combination of rapid heating with the application of high mechanical pressure leads to very fast densification at temperatures that, typically, are a few hundred degrees lower than in normal hot pressing. In SPS, the advantageous effects of the rapid consolidation have been demonstrated for both conductive and nonconductive powders.[247]

Due to the complex nature of various physical phenomena involved in SPS, the modeling of the process has been challenging and clear insights are only recently emerging.[226,248–253] Specifically, the SPS problem interconnects at least three different physical processes—the density of the sample determines the electrical behavior, which then controls the temperature distribution, and the temperature distribution governs the densification rate. Furthermore, in a real situation, the gradient in the density and hence the temperature and stress need to be taken into consideration.

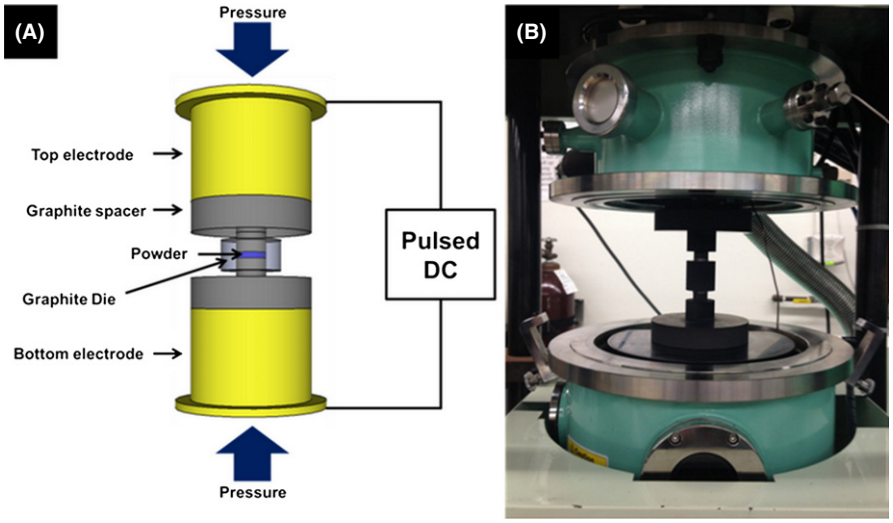

FIGURE 14 (A) Schematic representation of the SPS process, (B) SPS tooling before an experiment.[243] (Reprinted with permission from Elsevier)

Numerical modeling (primarily finite element) has been successful to simulate the temperature and electrical current distribution during SPS.[254–262] These analyses have been used to obtain temperature and stress distributions, which can then be used to predict densification using suitable constitutive properties. These simulations have also been used to optimize the SPS tool design.[261,263] The modeling of the stress and temperature distributions must be coupled with the constitutive parameters to obtain the densification of the sample. Most of the analyses have used the classical hot-pressing constitutive laws.[218,220] Using this approach, the overall shrinkage of the specimen has been simulated.[264,265] However, using the kinetics of the displacement of the electrode punches, only the average shrinkage rate is calculated, thereby neglecting the nonuniformity of the relative density within the specimen's volume. In addition, only a few investigators have developed and used SPS-specific constitutive models of powder consolidation.[248–250]

The nonuniform distribution of the relative density (porosity) under SPS is primarily caused by the nonuniformity of the temperature distribution as well as by the specifics of the mechanical boundary conditions (including punch-die geometry and friction at the specimen–tooling interfaces). However, as mentioned above, the nonuniform density distribution, in turn, influences the local thermal and electrical properties of the specimen, thereby rendering significantly different solutions of the SPS heat transfer and electric current density distribution problems. A significant step in addressing this complexity has been undertaken by including local density distribution in the framework of the finite-element models for the SPS process.[266–268] However, these studies have either considered only two-dimensional problems or have not properly accounted for densification in SPS condition (hot pressing in rigid die).

Researchers have only recently overcome the challenge of fully coupled 3D thermoelectromechanical analysis of the material processing under electric-current-assisted hot-pressing conditions (Figure 15). Using this approach, it was possible to conduct an analysis of the SPS net-shape capability and SPS scalability.[226,252,253,269] The developed modeling framework, however, incorporated the conventional models of hot pressing[218,220] and did not take into account the SPS-specific field-assisted constitutive mechanisms of material transport at multiple scales.

An outstanding question with significant arguments has been if there is an effect of the field, beyond rapid heating, on densification in SPS. One set of arguments has been that the only effect of the field is to provide fast heating, and therefore, SPS is similar to conventional hot pressing with an ultrafast heating rate. The other set of arguments contend that, in addition to a fast heating rate, the electrical field alters fundamental parameters that govern densification, eg, surface energy, chemical potential gradients, diffusion coefficients, wetting behavior (in systems with a liquid phase), or adds additional energy dissipative mechanisms, which should be included in the sintering constitutive equations (modification of Equation (7)). Due to the lack of a full theoretical analysis, this question has been primarily addressed experimentally. In this case, there are limitations as it is difficult, if not impossible, to reproduce the time–temperature profile of SPS in conventional thermal systems. A number of experimental studies have indicated that there is a SPS-specific nonthermal contribution to mass transport leading to accelerated densification.[239,270,271] On the other hand, from a series of carefully controlled experiments, using comparable heating rates, temperature, sample sizes, and applied stresses with those of hot-pressing, Langer and co-workers concluded that for Al_2O_3 (an insulator), yitira-stabilized ZrO_2 (an ionic conductor), and ZnO (a semiconductor), there was almost no

FIGURE 15 SPS die-punch set-up: photo (left); CAD model (middle); and 3D FE modeling of SPS processing (right). FE modeling shows nonuniformity of temperature distribution in SPS tooling[269]

other effect of SPS—just Joule heating leading to hot-pressing under rapid heating rate.[272–274] The authors, however, noted that all of their studies were conducted at low electrical fields (max ~15 V/cm) and there might be non-thermal effects at higher fields.

To clearly understand if, and under which conditions, there are nonthermal effects on densification in SPS, there is, therefore, a need for both carefully controlled experiments and multiphysics models.

4.2 | Microwave sintering

A microwave system typically consists of a generator to produce microwaves, a waveguide for their transport, a cavity to manipulate the microwave field, and a control system for tuning power and monitoring the temperature. A microwave field makes it possible to heat samples of any size and shape rapidly, uniformly, and efficiently. This characteristic of microwave heating can suppress grain growth. In addition to this microstructural benefit, low energy usage and cost are practical benefit of microwave sintering.

Microwave sintering has been used for over 50 years with significant research activities starting from the 1980s. Comprehensive reviews of the early development in microwave sintering showed that it can be used to efficiently sinter a wide variety of ceramics.[275,276] One of the early and distinguishing successes of microwave sintering was that it was used to make transparent sintered ceramics, indicating its potential to reach high density without significant grain growth.[277]

Direct comparison of conventional and microwave sintering for alumina has shown a much lower activation energy for microwave sintering than for conventional sintering.[278] As for the mechanisms responsible for enhanced sinterability in a microwave field, there are several hypotheses. These are associated with the so-called "microwave-effect" or non-thermal factors responsible for observed enhancements in sintering kinetics.[279] The prevailing theories are as follow:

1. Ponderomotive force interaction: It has been proposed that microwave-excited ionic currents become locally rectified (near the interface), giving rise to an additional driving force for mass transport.[279–282] Olevsky with co-authors have recently made progress determining the enhanced contributions of ponderomotive forces to microwave sintering densification[280] and interparticle contact growth.[282]
2. Acceleration of the grain-boundary diffusion by local noninsothermicity: Anisothermal heating generated in two different phases of widely varying microwave absorption characteristics can provide a strong driving force to cause enhancement in the reaction kinetics followed by sintering in reactive systems.[276,279,281] However, this explanation is applicable only to multiphase systems with selective heating.

Simulation of microwave sintering requires coupling of three physical phenomena: electromagnetism, heat transfer, and densification. Several groups have conducted finite-element simulations considering all of these coupled factors.[283–285] Recently, comprehensive 2D and 3D finite-element modeling of microwave sintering has been conducted by Maniere et al. and they have uncovered a noteworthy phenomenon of heating instability.[286,287] An example of the results from this simulation is shown in Figure 16.

4.3 | Flash sintering

"Flash sintering" is a term that was coined in 2010 by Raj and co-authors to describe ultra-rapid densification (in

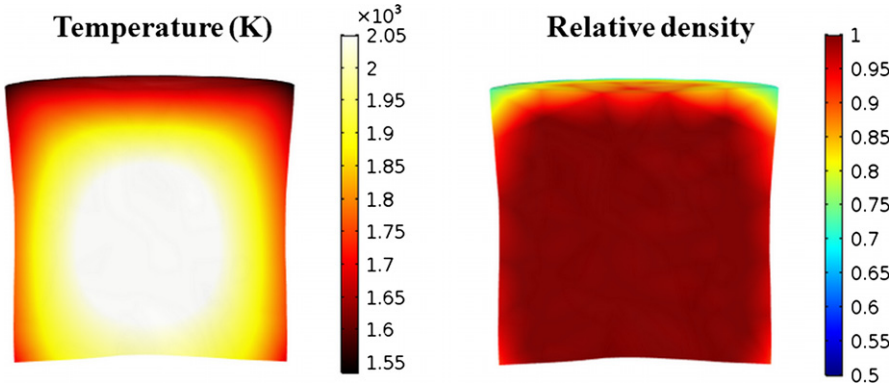

FIGURE 16 Evolution of temperature and relative density under microwave sintering of zirconia cylindrical specimen: Finite-element modeling indicating the phenomenon of hot spot formation. This phenomenon appears to be the reason of the instability of microwave sintering outcomes.[287] (Reprinted with permission from Wiley)

seconds) of ceramics.[288] Since then, it has been shown to be an effective technique to densify a variety of oxides to high density in an extremely short time.[288–293] In flash sintering, the green compact is connected to two electrodes and heated in a furnace to a critical temperature, and then a DC electric current is passed through the specimen using the electrodes. The applied voltage is usually of the order of 50–150 volts or higher, which is much greater than the voltage used in a typical SPS set up (<15 V).

Several explanations have been provided for the exceptionally rapid densification in flash sintering. The key challenge in the respective experiments continues to be accurate measurement of temperature and temperature gradients. The first set of explanations is based on the observation that, although due to the electric field and current the temperature rises, the increase is nowhere close to the necessary increase for this ultra-fast densification. The observed densification rate has been rationalized due to localized heating of the grain boundaries[288] or to mechanisms related to unstable avalanche of defects caused by a combination of electric field and temperature.[294] An alternative explanation, based on the observation of significantly higher sample temperatures,[295,296] is that Joule heating alone is responsible for thermal runaway, which is the most likely cause for rapid densification.[296,297] It is known that the electrical conductivity of many ceramic materials increases as temperature increases. Under a voltage-control regime, as used in flash sintering, the increase in the electric current, as temperature increases, leads to increased generation of Joule heat. This in turn causes a high increase in the specimen's temperature, leading to significantly higher sample temperature than the furnace temperature.[297]

Recently, a new ultrarapid process of flash spark-plasma sintering (Flash Hot Pressing—FHP) has been developed and demonstrated to sinter SiC.[298] The origin of this approach is in a detailed theoretical analysis of the thermal runaway effect in flash sintering and development of experimental approaches to address the challenge of uncontrollable thermal conditions. In FHP major concept is to stabilize the flash sintering process, through the application of external pressure. The effectiveness of the developed FHP technique was demonstrated by the consolidation of SiC powder, in a few seconds, in an industrial spark-plasma sintering device (Figure 17). Specially designed sacrificial dies heated the precompacted SiC powder specimen to a critical temperature followed by passing electric current. The experimental results demonstrate that flash sintering phenomena can be realized using conventional SPS devices. It is thus expected that this technique will be further explored as an important processing technique.[298]

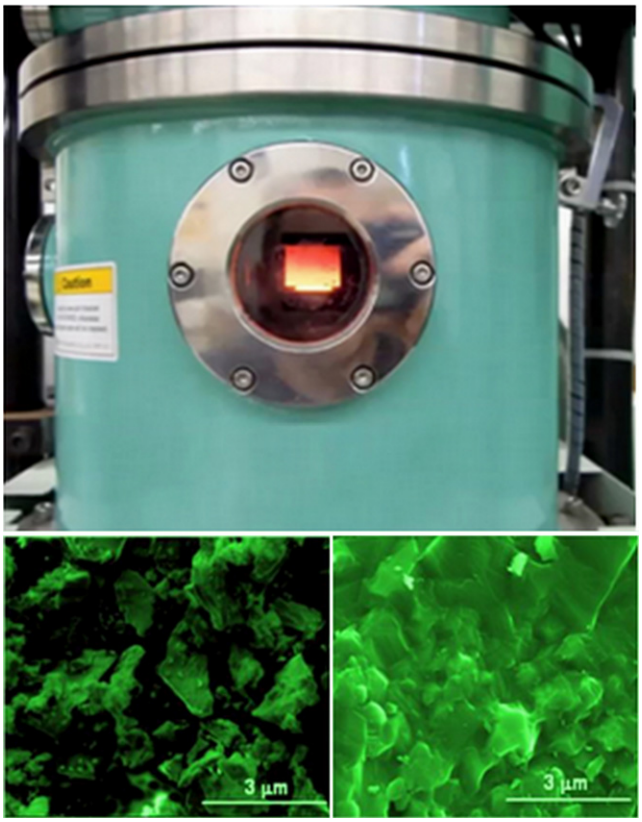

FIGURE 17 Top: Consolidation of silicon carbide at the moment of flash. Bottom: The SEM micrograph of SiC powder (left), and SiC specimen processed by flash SPS (right)[298]

4.4 | Sintering with thermal cycle modification

Thermal cycle engineering has been recognized as an efficient way to engineer the microstructure. Fast firing, which was developed by Harmer and Brook, is characterized by a much faster heating rate, a higher sintering temperature, and a shorter sintering time than those used in conventional sintering.[299] Fast fired samples have a smaller grain size for the same density and the technique is effective to suppress pore–boundary separation.[299,300] Fundamentally, this technique will be effective for any system where the activation energy of densification is higher than that of grain growth. This condition can be satisfied for most materials systems because the activation energies of lattice diffusion and grain-boundary diffusion along the boundary, for densification, are usually higher than that of grain-boundary diffusion perpendicular to the boundary for grain growth.[301] A fast heating rate is one of the most important contributors to efficient densification and grain growth control in other innovative sintering techniques, including spark-plasma sintering, microwave sintering, and flash sintering, as discussed in Sections 4.1–4.3.

Two-step thermal cycle techniques with combinations of a low and high temperature,[302,303] or a high and low temperature,[304,305] have been developed. The former, proposed by De Jonghe et al., introduces a presintering step, which can allow precoarsening of particles and suppression of locally uneven densification. This technique has been reported to be effective for several systems. The more recent two-step sintering technique with a high- and low-temperature combination, which was developed by Chen and Wang, consists of sintering for a short period of time at a temperature higher than the conventional sintering temperature, followed by rapid cooling to and sintering at a low temperature.[304] The effectiveness of this technique has been reported not only for solid-state sintering[305–307] but also liquid phase sintering.[308–311] However, the mechanism of grain growth suppression is as yet unclear. For solid-state sintered materials, grain growth suppression has been postulated to be a change in the dominant mechanism of grain growth with respect to temperature and relative density.[304,312] Separately, for two-step liquid phase sintering, the difference between the boundary mobilities with and without a liquid film at high and low temperature, respectively, was suggested to be the mechanism of grain growth suppression.[308,309] Recently, based on the measured grain size distributions and grain growth calculations for faceted systems, Kang et al. suggested that grain growth suppression, in particular, AGG suppression, was due to a reduction in the maximum driving force for the growth of the largest grain in the sample immediately after the first sintering step.[307,311] There is a need for additional research to clarify the mechanism(s) of grain growth suppression in the two-step sintering process.

4.5 | Sintering in a reactive atmosphere

The effect of the sintering atmosphere on densification and microstructural evolution has been investigated from many different viewpoints. One of the important effects of the atmosphere is that it becomes trapped in the pores in the final stage of sintering and has a critical effect on the final density that can be achieved. Coble showed that the sintering atmosphere determined the terminal density of sintered alumina and complete elimination of porosity was possible in hydrogen, oxygen, or vacuum but not in helium, argon, or nitrogen.[313] This phenomenon has been explained in terms of the increasing gas pressure in the closed pores due to pore shrinkage and reaching terminal density when the gas pressure in the pore balances the capillary pressure.[314] Another important effect of the atmosphere is that if the ambient gas reacts with the solid or if the solid has a high vapor pressure, then vapor transport can be a significant material transport pathway leading to coarsening of grains and a reduction in densification.[315–319] Atmosphere has also been shown to be important in controlling the structure of the grain boundaries, and this in turn has been shown to be critical in controlling grain growth.[47,48,117,119] For many metals, sintering can only be conducted in a reducing environment to ensure oxide-free pore surfaces.[13]

Hydrothermal processes have been well established as a powder synthesis technique. They have also been investigated as a low-temperature densification approach enhanced by reaction or solubility-related mass transport mechanisms. In the 1980s Yamasaki et al. developed a hydrothermal hot-pressing apparatus and showed that this apparatus can be used to sinter a broad range of ceramics, including silica and silicates, calcium carbonate, ZrO_2, and $BaTiO_3$ under mild conditions (temperature around 350°C and a pressure of 140 MPa).[320] Early developments in this field, reviewed by Somiya, included sintering up to a temperature of 1000°C and a pressure of 100 MPa.[321] After these initial studies, most of the focus of this line of investigations was on calcium-containing ceramics and the term "cold-sintering" was first coined.[322] In the last year, a series of publications by Randall et al. have shown that a wide variety of ceramics, including oxides, flourides, chlorides, iodides, phosphates, and carbonates, can be processed to fairly high densities under extremely mild conditions of 25–300°C and modest pressures (a few 100 MPa).[323–326] They have also used the term "cold sintering" and identified it as a low-temperature pressure-assisted liquid phase sintering in the presence of water.

5 | CHALLENGES AND OUTLOOK

In this section, we focus on a few overarching challenges and the outlook for significant progress in these areas.

5.1 | Predictive theory and modeling of sintering—multiscale simulation

As sintering is inherently an inverse problem, the overarching goal of the sintering theory is a predictive model that can describe the evolution of the density and shape of a sintering body if the powder characteristics, green state structure, and processing conditions are known. Although this is a daunting challenge, it should be noted that this problem has been solved for amorphous materials, as discussed in Section 2.3 for free sintering and in Section 3 for sintering of composites, constrained films, and stress-assisted sintering of amorphous materials. The challenge is to realize this level of predictability for SSS and LPS materials.

Sintering is fundamentally characterized and controlled by phenomena occurring at multiple length scales.[13,15–17,327] At the smallest scale, electronic and atomic length, for example, temperature, atmosphere, and dopants, control the diffusion coefficients, as well as surface and grain-boundary energies. Progress in simulations and measurements of these parameters has been extremely limited for ceramics and is an area that warrants significant attention. Beyond the small length scale, the next two length scales, the mesoscale (the length scale of particles, grains, and pore) and the continuum scale (component level), have features unique to sintering systems. The challenges and the outlook for the mesoscale simulation are discussed in Section 5.2. Here, we focus on multiscale simulations.

The theories and simulations of sintering systems (an ensemble of particle or pore/grain system) have focused on (i) mesoscale simulation using physical models, and (ii) use of experimentally derived parameters in macroscopic models. The mesoscale theories have helped establish the physical basis of the observed phenomenon in sintering (Section 2). However, the predictable capability of these theories has been limited, in part due to the use of ideal simple geometries (eg, two-particle system) or to simplifying assumptions about the kinetic process (eg, densification without grain growth). The macroscopic theory and simulation was discussed in Section 3 for complex sintering problems. As highlighted in that section, the required constitutive parameters have been experimentally obtained and, as was also highlighted, there is a need to use simulated parameters.

There is thus need to first develop robust approaches for mesoscale simulations of realistic particle packing and pore/grain microstructures and, second, to combine the above-mentioned two approaches (physically based and phenomenological) to predict the evolution of realistic microstructures coupled with a technologically important macroscopic analysis. As discussed in Section 5.2, there are promising recent developments in understanding and simulation of mesoscale structure evolution during sintering. Constitutive models of sintering used in finite-element computer codes should be refined taking into consideration specifics of real grain structures.

For real sintering simulations, it is necessary to develop an approach that can treat in detail both the evolution of a realistic mesostructure and the sintering mechanisms of a realistic powder compact. For this purpose, as shown in Figure 18, the stereological theory of sintering can be incorporated into a lattice-based, kinetic Monte-Carlo (kMC) model, also known as the Potts model (see Section 5.2). The stereological theory of sintering describes the evolution of individual stereological constructs such as the grain boundary and pore–grain interface for the given mass transport mechanisms. However, it cannot track the changes at all such boundaries in a complex topology. Incorporation of the stereological model into the Potts model allows tracking of microstructural changes in a complex and realistic geometry.

In modeling of sintering, two approaches to link different hierarchical scales (eg, meso- and macro-) are possible. The first focuses on direct determination of the macroscopic constitutive parameters based on the mesoscale simulations. This approach has been implemented by Olevsky et al.[136] In the second approach, the computational finite-element framework at the macroscopic level includes

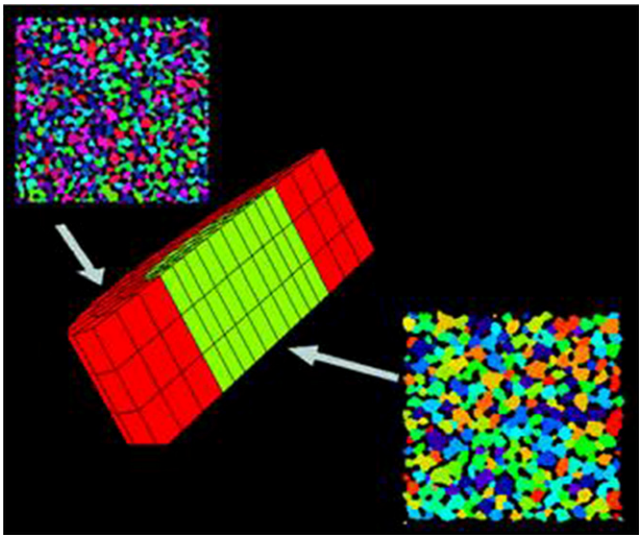

FIGURE 18 Multiscale (meso–macro) modeling of the sintering of a cylindrical powder body with a cylindrical inclusion. The macroscale finite-element calculations predict shape evolution and relative density distribution in the macroscopic specimen. The mesoscale kMC calculations predict pore–grain structure evolution in each finite element

mesoscopic simulators.[328,329] An example, using the first approach, is illustrated in Figure 18, which is a simulation of the sintering of a cylindrical powder body with a cylindrical inclusion. Each element of the macroscopic finite-element code also represents a domain for the simultaneous mesoscale kMC calculation of the evolution of the pore–grain structure inside the element. The image shown in Figure 18 represents the parallel solution of the macroscopic problem of the sintering with an inclusion (in terms of the shape distortion and relative density spatial distribution) and the mesoscopic problem of the pore–grain structure evolution (shown for two representative finite elements chosen inside the matrix and the inclusion, respectively.)

Different length scales commonly cause difficulties in the correlation of time scales. For kMC calculations, no physical time is utilized—the simulations are conducted in terms of the "Monte-Carlo time steps". To transfer the data between the meso- and macroscales, it is necessary to correlate physical and conventional times. In publications of Bordere et al.[330,331] this is accomplished through a generic dimensional analysis, whereas in the works of Olevsky et al.[136] the correlation is achieved by comparing physical and conventional time scales at the same characteristic porosity level calculated by independent mesoscale simulations and macroscale modeling. The validity of these approaches and their implementation needs further investigations.

5.2 | Mesoscale simulations of sintering

Microstructural evolution during sintering has been studied starting from the late 1940s.[7-23] In these studies, idealized powder compacts consisting of 2 or 3 spherical particles (or pores) of equal size, sintered by various diffusion mechanisms, were considered. These early models were critical in establishing the physical basis of sintering of amorphous and crystalline materials including the driving forces, transport mechanisms, and densification processes. Next, periodical unit cells of the same geometry were utilized. Examples of these include, the models of Scherer[123] and Mackenzie-Shuttleworth[124] for viscous sintering, the stereological model of DeHoff,[332] the particle network models of Bouvard and McMeeking,[333] and intermediate- and final-stage models from Riedel and co-workers.[158,334] In these models, each repeating cell consists of a matrix (solid phase) and the voids embedded in it. The intermediate sintering stage, where the solid and porous phase are interconnected, and the final sintering stage, where pores become isolated, could be described in a more detailed fashion in terms of the shapes of grains and pores based on these models. In addition, some of these idealized geometric simulations have been used to obtain the sintering stress necessary for modeling sintering at the continuum level.[123,158,333]

In addition to these analytical approaches, many numerical simulations have been conducted in the past 20–25 years to investigate the sintering kinetics and microstructural evolution. Molecular dynamics has been used to study early-stage sintering of nanoparticles.[335–339] These simulations provided novel insights, including additional mechanisms such as particle rotation for nanoscale particulate systems. Very accurate particle shape evolution and sintering kinetics models have been developed using continuum mechanics methods for the sintering of two,[340] three,[341] and a row[342] of particles. Another very effective approach of using the surface evolver technique has been introduced by Wakai and co-workers for sintering calculations of several particles. This approach has been used to calculate sintering stresses,[150,343] anisotropic sintering stresses,[233] densification kinetics,[344] kinetics of the closure of a pore surrounded by three particles,[345] anisotropic shrinkage rates and viscosities,[346] and the effect of constraint and external stresses on the microstructural evolution.[234]

Discrete-element simulation (DES) is another powerful approach that recently has been introduced to study the microstructural evolution during early and intermediate stages of sintering (density from initial packing density to 85–90% of theoretical density).[347,348] DES provides a practical way to consider particle rearrangement because the force equilibrium is calculated for each individual particle or discrete element. These simulations use a large number of particles to obtain realistic microstructures. Comparisons with experimental data have shown good agreement regarding the evolution of the contact area between particles and volume shrinkage.[347,348] The most significant contribution of DES has been to investigate complex sintering problems. For example, DES was used to simulate the evolution of anisotropic microstructure due to uniaxial stress.[231] In this study, the anisotropic shrinkage was calculated and compared well with the experimental results. Another example of the simulation of complex sintering problems is the simulation of constrained sintering.[205] The simulations[204,205] showed that the pores become anisotropic and preferentially oriented near the substrate, as has been observed experimentally.[203] DES has also been used to simulate the evolution of defects in constrained sintering.[209] One result from these simulations is shown in Figure 19. As shown in this figure, this study highlighted the importance of interparticle sliding resistance (η_{part}). It is shown that defects are more likely to form in constrained sintering films in which η_{part} is high and less likely in systems with low η_{part}. This may explain the long-standing experimental observation that constrained sintering cracks form more easily in crystalline films than in amorphous films.[206] However, this hypothesis (role of interparticle sliding resistance) needs to be experimentally verified. Finally, DES has, recently, been used to simulate sintering

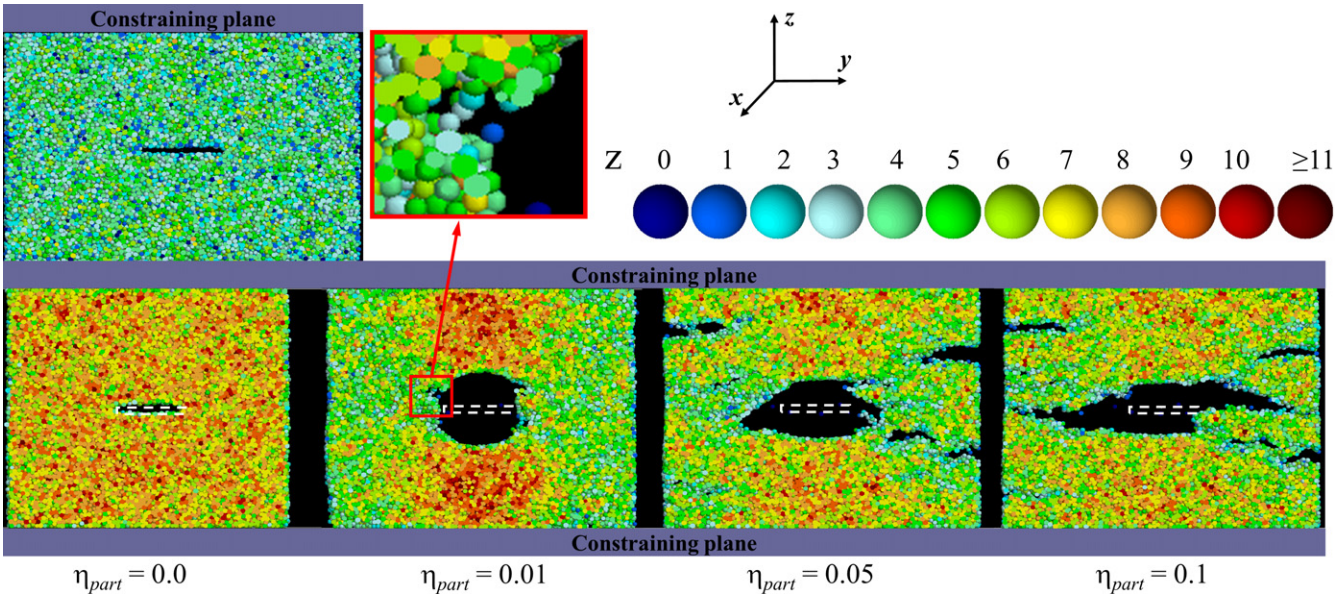

FIGURE 19 Discrete-element simulation of constrained sintered films. Section of the initial (top) and final (bottom) microstructures of a constrained sintered film with a crack for different values of interparticle sliding resistance, η_{part}. Color indicates the coordination number of the particles which correlates well with local density. The white rectangle is the initial location and size of crack. The close-up view of the second picture shows a small crack at the periphery of the main crack. Defect more likely in films with higher η_{part}.[209] (Reprinted with permission from Wiley)

of hierarchical porous ceramics, sintering of composites, and the effect of green packing on densification.[349] In all cases, the qualitative predictions match well with experimental observations. There is a need for careful quantitative comparison of experimental results with these simulations. In addition, DES has been used to calculate the properties of partially sintered bodies. As DES predicts the grain size and its distribution quite well, excellent agreements have been found in the simulated and measured elastic properties,[350] fracture toughness,[351] compressive strength,[352] and transport properties.[353] The DES approach can be used to calculate the constitutive parameters and should be extended to predict anisotropic constitutive parameters (Section 3.5).

All of the above-mentioned numerical simulations have significantly advanced the understanding of sintering. However, with the exception of the molecular dynamics and the discrete element, they are still far from being a true mesoscale simulation of sintering, as only a limited number of particles (or grains) are considered. The discrete element and molecular dynamic-based calculations consider larger numbers of particles: however, they often operate with particles of idealized (mostly spherical) shape. In addition, these approaches are not able to simulate grain–pore interaction during grain growth.

The application of Monte-Carlo methods to sintering problems is another powerful mesoscale simulation approach. They have been used to simulate final-stage sintering using realistic microstructural features (grains and pores) and kinetic parameters (diffusivities and boundary mobilities). The simulations accurately reproduce theoretically predicted sintering kinetics and the observed evolution of the microstructures including pore shrinkage, grain growth, pore breakaway, and reattachment.[354] Olevsky and Tikare used a mesoscale unit cell of hundreds of realistic-shape particles as a basis for a kinetic Monte-Carlo model to simulate sintering.[136,355–357] Figure 20 is an example of results from this approach. The calculation results reproduce the dynamics of grain growth, pore collapse, and the overall shrinkage of the system. In KMC simulation, as

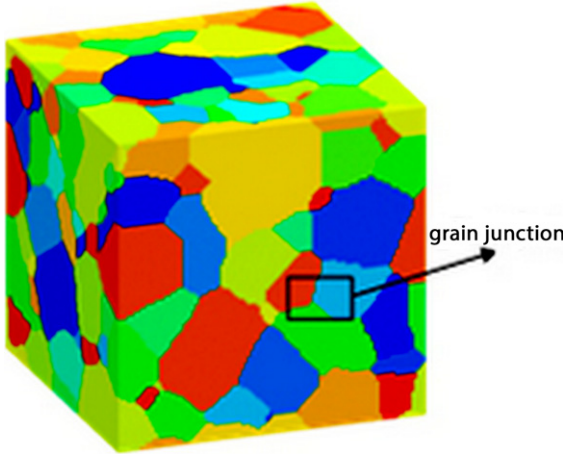

FIGURE 20 Kinetic Monte-Carlo mesoscale simulation of grain growth and grain structure during final stages of sintering. Colors correspond to grain orientations. (Courtesy of Dr. V. Tikare)

only a few assumptions are needed for the geometry of the particles and their evolution during sintering, it allows us to obtain more general thermodynamic (eg, sintering stress and bulk viscosity) and kinetic data (eg, densification rate) for sintering.

5.3 | Interface structure and microstructural evolution during sintering

The interaction between grains and pores, although long studied, remains a fundamental challenge in sintering science and is the primary reason that the densification behavior of crystalline materials is not as well predicted as the densification behavior of amorphous materials. Recent studies on densification and grain growth in porous ceramics, in particular, for solid-state sintering, demonstrated critical effects of the interface structure.[40,49,53,54,61] Various implications of interface structure on densification kinetics and microstructural evolution remain and should continue to be an active area of research. For example, the observed limit of densification in some SSS and the varieties of microstructural evolution in the same SSS system have been ascribed to the nonlinear kinetics of atom transport with respect to the driving force for systems with faceted boundaries.[41,47,53,54] In these studies, average thermodynamic and kinetic properties were assumed to be operative. In reality, however, as the atomic structure is different from boundary to boundary, the reaction rate at the boundary and the resulting kinetics are different for different boundaries under the same driving force. In this respect, fundamental and detailed studies on individual boundaries, as well as an ensemble of boundaries, should be performed for better understanding of the boundary structure effect on boundary kinetics and sintering. They may include (i) the atomistic characterization and calculation of the grain-boundary structure, (ii) the atomistic observation and calculation of the boundary structural transition, (iii) model and theory of atomistic motion along and across boundaries, (iv) a theory of densification with respect to the boundary structure, including vacancy annihilation, (v) simulation of microstructural evolution in faceted systems, and (vi) experimental and theoretical studies on the effects of other parameters, such as impurities, second-phase particles, and defects, on densification, grain-boundary structure, and grain growth. The ultimate goal of these studies would be the prediction of sintering kinetics and microstructural evolution in polycrystalline ceramics with a precision similar to that of the sintering of amorphous powder compacts.

5.4 | Sintering of nanopowders

Sintering of nanoparticle materials requires much greater control over particle packing homogeneity, grain growth, and densification than what is currently possible. This is because nanoparticles agglomerate easily and exhibit much faster grain growth than micrometer-sized particles due to their very high specific surface area. Multiscale, quantitative, and integrated understanding of nanostructural sintering evolution is of significant importance. Currently, there are several hurdles to achieving this goal.

A distinctive structural characteristic of nanomaterials is the presence of agglomerates, either inherited from the stage of powder synthesis or developed due to the instability of consolidation. Early in the investigation of sintering, agglomerates were shown to modify densification, for example,[358] and they can lead to processing defects during sintering.[173,174,181] Principal steps of a consistent modeling approach should embrace all the main stages and aspects of consolidation, including synthesis of particles and formation of agglomerates, deformation of agglomerates, densification of powders with agglomerates, and macroscopic deformation of nanostructure materials with agglomerates.

The analysis of the agglomerated structure evolution during densification substantially differs from the traditional sintering as the powder compact with agglomerates has at least two distinctly different pore sizes. This hierarchical pore size can lead to interesting and unexpected effects. For example, it has been recently shown that during sinter-forging, large pores orient perpendicular to the applied compressive stress while small pores orient parallel to the applied stress.[230] Proper multiscale simulations of this observation are currently underway. Agglomeration leads to nonuniform densification of nanopowders which modifies the overall densification behavior and can generate processing defects, as discussed in Section 3.2. The grain growth behavior in agglomerates is also expected to be different from that in the matrix and this could intensify the tendency for AGG. Finally, agglomerates and bimodal pore sizes would affect the continuum properties such as the sintering stress and viscosity.

In addition to the above-mentioned issues related to agglomeration for nanoparticle sintering, the correlation between grain growth and densification has its own specific features. Some of these, including the particulars of pore pinning of grain boundaries and the influence of triple junctions (suggested as a basis for the two-stage sintering concept), have been investigated.[359] These effects need to be carefully evaluated experimentally. Finally, the level of sintering stress in nanopowder sintering, which is inversely proportional to the particle radius, can reach levels corresponding to the nonlinear mechanisms of mass transport, such as power-law creep.[360] This nonlinearity may affect not only the kinetics of mass transport but also the driving force, and hence the sintering stress may become dependent on the material's strain rate sensitivity.[360]

Due to the increasing ability to make a variety of nano-sized particles and specific advantages of nanostructured materials, there will be continued interest in the investigation of the densification and microstructural evolution of nanopowders.

5.5 | Additive manufacturing using selective laser sintering

Additive manufacturing (AM) encompasses a wide group of different approaches based on layer-by-layer fabrication of components. This field is rapidly growing and comprises many processes.[361,362] An important process that starts with powder is selective laser sintering. In this process, selected areas in a powder bed are sintered using a high power laser.[361] This is an important approach for AM of metallic materials.[363,364] In many cases, the metal particles partially melt and the sintering should be viewed as liquid phase sintering. However, compared with the conventional LPS, there are additional complications because of its dynamic, transient, and nonequilibrium nature. Studies on selective laser sintering of ceramics are rather limited.[365–367] Furthermore, selective laser sintering has limitations for ceramics due to the low thermal conductivity of ceramics and the longer time required for sintering.[368] Nevertheless, this field is expected to grow because of its versatility and convenience in making components of complex shapes. For the growth of ceramics AM, there are needs for further understanding of the interaction between laser and ceramic powders, sintering under thermal gradients, and classical issues such as constrained and composite sintering applied to layer-by-layer laser sintering.[368]

5.6 | Damage and fracture criteria for sintering bodies

Although significant work has been done to predict and understand the strength of dense materials, the damage and failure criteria for porous ceramics under sintering conditions have not been investigated adequately. Research should be focused on the development of damage growth and failure criteria, which can then be integrated with continuum simulation which calculate internal stresses in sintering bodies (eg, sintering of composites or constrained sintering). Furthermore, the integrated approach of modeling and experiments should provide the basis for online process control for a wide range of sintering operations so that dynamic changes in the process conditions can be made to avoid failure.

The evolution of the strength of a particulate material during sintering is an important characteristic in powder processing. Despite the intensive development of sintering models, presently, the main information that can be obtained from modeling is data on dimensional change, stress–strain conditions, and the porosity (density) distribution. The engineering strength of powder components during sintering is also of considerable importance, for the analysis of, for example, crack nucleation and formation during sintering. In general, the prediction of failure and damage is of utmost significance in sintering practice. With respect to damage, in the development of sintering models, it should be recognized that the early stage of sintering is the most critical stage because the powder compact is weakest in this stage. However, during the early stage, density is not a good state variable as neck growth, which increases the compact strength, can take place without significant change in density. An additional complication to be considered is that in most sintering situations, failure may not be brittle but rather due to time-dependent (creep crack growth) damage accumulation and growth. There have been some developments in this area but the topic remains open for significant and comprehensive investigations.[153,182,206,352,369,370]

5.7 | Development of optimization approaches—predictable shape changes

Sintering of macroscopically inhomogeneous powder components is always accompanied by shape distortion due to the difference in shrinkage rates of powder elements. An objective of sintering optimization is the theoretical determination of for near-net-shape fabrication of components from initially distorted green bodies. To predict the initial shape of the component that will result in the final desired shape and size, the "reverse" numerical procedure can be used, adopting the assumption that the component swells from the final shape to the initial shape under the influence of pressure equal to the sintering stress (but of opposite sign).

A possible numerical approach for the prediction of the initial shape of a component is based on a finite-element implementation of the continuum theory of sintering. From the macroscopic point of view, shrinkage during sintering can be treated as a linear creep of a porous body under the influence of the internal compressive pressure, which is usually termed as "sintering stress" or "Laplace pressure", as discussed in Section 3.1. If the initial shape and composition of a powder body are known, the theory of sintering can predict its final shape. Conversely, for the problem of optimizing the initial shape, the final shape of a component is known and the initial shape has to be found. It seems natural to consider the "reverse" process of swelling of the component from the final to the initial shape under the influence of the "negative sintering pressure".

Using the above-mentioned approach, the initial shape corresponding to a certain level of the mean initial density can be readily found, but realistically, the initial density

will be distributed nonuniformly in the volume. To obtain the initial shape of a green body with a nonuniform density distribution, an iterative procedure should be used. This approach was used for the prediction of optimum initial shapes of powder components during hot isostatic pressing or sintering of functionally graded composites.[371,372] This procedure can be applied only when the sintering stress and the constitutive behavior of the powder body are known.

Another important area that requires application of optimization methodologies is the selection of sintering temperature regimes. The expected progress in theory and multiscale modeling of ceramics as outlined above should lead to progress in fundamental and routine use of this inverse approach to optimize the green state and the thermal profile to make ceramics of desired shape, density, and microstructure with minimum processing rejections and limited experiments.

5.8 | Other challenges and opportunities

In addition to the major challenges and opportunities summarized above, here we outline some other challenges and opportunities for further development of sintering science and technology.

1. Factors of a nonthermomechanical nature generally are not incorporated into current sintering models. Such factors include but are not limited to phase transformations, chemical reactions, influence of sintering atmospheres, oxidation, etc.
2. For constrained multilayered sintering, intermediate levels of constraint need to be systematically investigated as it is clear that in most practical situations, the films are not fully constrained. In addition, the finite geometry aspects have not been investigated comprehensively. As all films have finite geometry, the effects of film/substrate size, free edge effects, aspect ratio of patterned films, and film/substrate thickness ratio should be investigated. This topic will also be very relevant for additive manufacturing.
3. Integrated experimental and multiscale simulations studies are required to increase the practical utility of simulations. This is the case for many problems. An example is the complementary studies of experimental and discrete-element simulations for anisotropic systems. Well calibrated (using experimental results) discrete-element simulations could be used to derive anisotropic constitutive parameters, which are difficult to obtain experimentally. These constitutive parameters could then be used in finite-element simulations to simulate important effects (eg, stress distribution in constrained sintering finite geometry films).

6 | SINTERING PRACTICE

The sintering theory developed over the last six decades and summarized above has led to an understanding of the effects of critical parameters on densification and final microstructure. Many important lessons have been learned and implemented in practice.[13-17] Some important points are summarized below.

It has been recognized that the control of the green compact is particularly important in sintering practice.[373] It has been shown that high and uniform green density is desirable and strategies including controlled particle size distribution have been implemented to improve green density and sintering behavior.[374] The powder should be nonagglomerated, equiaxed, and of high purity or controlled dopant level.[12-17] These requirements have led to the development of chemical techniques to produce ceramic powders of high purity and controlled size. In addition, emphasis has been placed on green state processing, in particular ways to avoid agglomeration using colloidal processing.[375] Using the sintering science as a guide, Yan identified the desired conditions for good microstructural control during densification.[315] In addition to the desired characteristics of the green compact, which were highlighted above, the other important factors are as follows: dopant level, sintering atmosphere, and firing schedule. Although each of these must be optimized for a specific system, some general guidelines are clear. Basically, the nondensifying (i.e., the coarsening) mechanisms should be suppressed and the densifying mechanisms should be promoted. Therefore, it is desirable to find the species and the amount of dopants, the sintering atmosphere, and the heating schedule that favor grain-boundary diffusion along the boundary and/or volume diffusion over grain-boundary diffusion perpendicular to the boundary, surface diffusion, and vapor transport. In addition, the conditions that minimize exaggerated grain growth (so that pores are not trapped in the grain in the final stage) are favored. To ensure the general guidelines, several strategies have been devised, including controlling the grain-boundary structure by using dopants and a suitable atmosphere, and the use of a second phase (in some cases transient) to pin grain boundaries. The importance and the effect of thermal cycle have been discussed in Section 4.4 and the effect of the atmosphere has been addressed in Section 4.5.

7 | SUMMARY

Sintering is an important approach to manufacture ceramics and hard metals of controlled density and microstructure. It is used for a broad range of applications from pottery to high technology modern ceramics. In the last seven

decades, our understanding of the sintering science and technology has advanced considerably.

This manuscript provides an overview of these advances. The basics including the thermodynamics and kinetics of sintering have been presented. The various models for sintering of powder compacts in different geometric stages have been discussed for different types of sintering (solid state of crystalline and amorphous ceramics and liquid phase). We also summarized some of the important areas of current research, including the effects of interface structure on sintering, sintering of multicomponent materials, sintering of multilayered systems, sintering under external stresses, field-assisted sintering, microstructure-based models, and multiscale models.

Although considerable progress has been made, multiple areas of active sintering research remain. In addition to the emerging areas, such as constrained sintering, field-assisted sintering, and additive manufacturing, the precise quantitative description of sintering is an active direction of research and development. It has been shown that microstructure-based models and multiscale modeling are promising approaches. Important lessons from the science of sintering have been and are expected to be applied to the sintering practice of numerous technologically important materials and systems.

ACKNOWLEDGMENT

RKB and EAO acknowledge partial support during the writing of this manuscript from the US National Science Foundation Division of Civil and Mechanical Systems and Manufacturing Innovations for this collaborative DMREF project (NSF Grant nos. CMMI 1502392 and CMMI 1234114). Mr. Gi-Young Jo is acknowledged for his assistance during the preparation of the manuscript.

REFERENCES

1. Ferguson JB. Note on the sintering of magnesia. *J Am Ceram Soc*. 1918;1:439-440.
2. Bordia R, Olevsky E. Advances in sintering science and technology. *J Am Ceram Soc*. 2009;92.
3. Bordia RK, Olevsky EA. *Advances in Sintering Science and Technology: Ceramic Transactions*. Hoboken, NJ: Wiley; 2009.
4. Kang SJL, Bordia RK, Bouvard D, et al. Advances in sintering research. *J Am Ceram Soc*. 2012;95:2357.
5. Kang SJL, Bordia RK, Olevsky EA, et al. *Advances in Sintering Science and Technology II: Ceramic Transactions*. Hoboken, NJ: Wiley; 2012.
6. Kieback B, Bordia RK, Bouvard D, et al. Preface. *J Am Ceram Soc*. 2015;98:3423.
7. Walker RF. Mechanism of material transport during sintering. *J Am Ceram Soc*. 1955;38:187-197.
8. Huppmann WJ. Sintering in the presence of liquid phase. In: Kuczynski GC, eds. *Chapter 27 in Sintering and Catalysis*. New York, NY, NY: Springer, Plenum Press; 1975:359-378.
9. Coble RL, Cannon RM. Current paradigms in powder processing. In: Palmour H, Davis RF, Hare TM, eds. *Chapter 14 in Processing of Crystalline Ceramics*. New York, NY: Springer, Plenum Press; 1978:151-170.
10. Exner HE, Petzow G. A critical evaluation of shrinkage equations. In: Kuczynski GC, eds. *Chapter 8 in Sintering Processes*. New York, NY: Springer, Plenum Press; 1980:107-120.
11. Exner HE, Arzt E. Sintering Processes. In: Cahn RW, Hassen P, eds. *Chapter 30 in Physical Metallurgy*, 3rd edition. Elsevier Science Publication, AM; 1983:1885-912.
12. Dynna GM, Chiang YM, Sintering of Advanced Ceramics. In: Handwerker CA, Blendell JE, Kaysser WA, eds. *Vol. 7 in Ceramics Transactions*. Westerville, OH: American Ceramic Society, 1990:547-61.
13. German RM. *Sintering Theory and Practice*. New York, NY: John Wiley & Sons; 1996.
14. German RM, Messing GL, Cornwall RG. *Sintering Technology*. New York, NY: Marcel Dekker Inc.; 1996.
15. Kang SJL. *Sintering: Densification, Grain Growth and Microstructure*. Oxford: Elsevier Butterworth-Heinemann; 2004.
16. Rahaman MN. *Sintering of Ceramics*. New York, NY: CRC Press; 2007.
17. Fang ZZ. *Sintering of Advanced Materials*. Cambridge: Woodhead Publishing Ltd.; 2010.
18. Frenkel J. Viscous flow of crystalline bodies under the action of surface tension. *J Phys*. 1945;9:385-91.
19. Pines BY. On sintering in the solid phase. *Zh Tekh Fiz*. 1946;16:737-745.
20. Coblenz WS, Dynys JM, Cannon RM, et al. Initial stage solid state sintering models. A critical analysis and assessment. *Mater Sci Res*. 1980;13:141-157.
21. Burke JE. Role of grain boundaries in sintering. *J Am Ceram Soc*. 1957;40:80-85.
22. Coble RL. Sintering crystalline solids. I. Intermediate and final state diffusion models. *J Appl Phys*. 1961;32:787-792.
23. Johnson DL. A general model for the intermediate stage of sintering. *J Am Ceram Soc*. 1970;53:574-577.
24. Zhao J, Harmer MP. Sintering kinetics for a model final-stage microstructure: a study of Al_2O_3. *Phil Mag Lett*. 1991;63:7-14.
25. Kang SJL, Jung YI. Sintering kinetics at final stage sintering: model calculation and map construction. *Acta Mater*. 2004;52:4573-4578.
26. Ashby MF. A first report on sintering diagrams. *Acta Metall*. 1974;22:275-289.
27. Swinkels FB, Ashby MF. A second report on sintering diagrams. *Acta Metall*. 1981;29:259-281.
28. Herring C. Effect of change of scale on sintering phenomena. *J Appl Phys*. 1950;21:301-303.
29. Alexander BH, Balluffi RW. The mechanism of sintering of copper. *Acta Metall*. 1957;5:666-677.
30. Kingery WD, Francois B. Sintering of crystalline oxides: I, interactions between grain boundaries and pores. In: Kuczynski GC, Hooten NA, Gibbon CF, eds. *Sintering and Related Phenomena*. NewYork, NY: Gordon & Breach; 1967:471-496.
31. Brook RJ. Pore-grain boundary interactions and grain growth. *J Am Ceram Soc*. 1969;52:56-57.
32. Hsueh CH, Evans AG, Coble RL. Microstructure development during final/intermediate stage sintering—I. pore/grain boundary separation. *Acta Metall*. 1982;30:1269-1279.

33. Sakarcan M, Hsueh CH, Evans AG. Experimental assessment of pore breakaway during sintering. *J Am Ceram Soc*. 1983;66: 456-461.
34. Zhao J, Harmer MP. Effect of pore distribution on microstructure development: I, matrix pores. *J Am Ceram Soc*. 1988;71:113-120.
35. Riedel H, Svoboda J. A theoretical study of grain growth in porous solids during sintering. *Acta Metall Mater*. 1993;41:1929-1936.
36. Handwerker CA, Cannon RM, Coble RL, Final-stage sintering of MgO. In: Kingery WD, eds. *Vol. 10 in Advances in Ceramics*. Columbus, OH: American Ceramic Society, 1985:619-643.
37. Zhao J, Harmer MP. Effect of pore distribution on microstructure development: II, first-and second-generation pores. *J Am Ceram Soc*. 1988;71:530-539.
38. Rödel J, Glaeser AM. Pore drag and pore-boundary separation in alumina. *J Am Ceram Soc*. 1990;73:3302-3312.
39. Kwon ST, Kim DY, Kang TK, et al. Effect of sintering temperature on the densification of Al_2O_3. *J Am Ceram Soc*. 1987;70: C69-70.
40. Choi SY, Kang SJL. Sintering kinetics by structural transition at grain boundaries in barium titanate. *Acta Mater*. 2004;52:2937-2943.
41. Lee MG, Chung SY, Kang SJL. Boundary faceting-dependent densification in a $BaTiO_3$ model system. *Acta Mater*. 2011;59:692-698.
42. Kang SJL. Sintering. In: Riedel R, Chen IW, eds. *Chapter 6 in Ceramics Science and Technology*. Weinheim: Wiley-VCH Verlag & Co. KGaA; 2012:141-169.
43. Lee BK, Chung SY, Kang SJL. Grain boundary faceting and abnormal grain growth in $BaTiO_3$. *Acta Mater*. 2000;48:1575-1580.
44. Park CW, Yoon DY. Effects of SiO_2, CaO_2, and MgO additions on the grain growth of alumina. *J Am Ceramic Soc*. 2000;83: 2605-2609.
45. Koo JB, Yoon DY. The dependence of normal and abnormal grain growth in silver on annealing temperature and atmosphere. *Metall Mater Trans A*. 2001;32:469-475.
46. Cho YK, Kang SJL, Yoon DY. Dependence of grain growth and grain-boundary structure on the Ba/Ti ratio in $BaTiO_3$. *J Am Ceram Soc*. 2004;87:119-124.
47. Jung YI, Choi SY, Kang SJL. Effect of oxygen partial pressure on grain boundary structure and grain growth behavior in $BaTiO_3$. *Acta Mater*. 2006;54:2849-2855.
48. Fisher JG, Kang SJL. Microstructural changes in $(K_{0.5}Na_{0.5})NbO_3$ ceramics sintered in various atmospheres. *J Eur Ceram Soc*. 2009;29:2581-2588.
49. An SM, Kang SJL. Boundary structural transition and grain growth behavior in $BaTiO_3$ with Nd_2O_3 doping and oxygen partial pressure change. *Acta Mater*. 2011;59:1964-1973.
50. Chen Z, Peng F. Normal and abnormal grain growths in $BaTiO_3$ fibers. *J Am Ceram Soc*. 2014;97:2755-2761.
51. Jung SH, Kang SJL. Repetitive grain growth behavior with increasing temperature and grain boundary roughening in a model nickel system. *Acta Mater*. 2014;69:283-291.
52. An SM, Yoon BK, Chung SY, et al. Nonlinear driving force–velocity relationship for the migration of faceted boundaries. *Acta Mater*. 2012;60:4531-4539.
53. Kang SJL, Lee MG, An SM. Microstructural evolution during sintering with control of the interface structure. *J Am Ceram Soc*. 2009;92:1464-1471.
54. Kang SJL, Ko SY, Moon SY. Mixed control of boundary migration and the principle of microstructural evolution. *J Ceram Soc Jpn*. 2016;124:259-267.
55. Kang SJL, Park JH, Ko SY, et al. Solid-state conversion of single crystals: the principle and the state-of-the-art. *J Am Ceram Soc*. 2015;98:347-360.
56. www.ceracomp.com
57. Deep Market Research Report on Global Piezoelectric Ceramics Industry. OY Research Group. New York, USA, 2015.
58. Dillon SJ, Tang M, Carter WC, et al. Complexion: a new concept for kinetic engineering in materials science. *Acta Mater*. 2007;55:6208-6218.
59. Dillon SJ, Harmer MP. Diffusion controlled abnormal grain growth in ceramics. *Mater Sci Forum*. 2007;558–59:1227-1236.
60. Harmer MP. Interfacial kinetic engineering: how far have we come since kingery's inaugural sosman address? *J Am Ceram Soc*. 2010;93:301-317.
61. Bäurer M, Shih SJ, Bishop C, et al. Abnormal grain growth in undoped strontium and barium titanate. *Acta Mater*. 2010;58: 290-300.
62. Harmer MP. The phase behavior of interfaces. *Science*. 2011;332:182-183.
63. Cantwell PR, Tang M, Dillon SJ, et al. Grain boundary complexions. *Acta Mater*. 2014;62:1-48.
64. Abbruzzese GC, Buccioni M. Theory of grain growth in the presence of atoms drag effects. *Mater Sci Forum*. 2007;558–59:1005-1012.
65. Kim SG, Park YB. Grain boundary segregation, solute drag and abnormal grain growth. *Acta Mater*. 2008;56:3739-3753.
66. Rollett AD, Srolovitz DJ, Anderson MP. Simulation and theory of abnormal grain growth—anisotropic grain boundary energies and mobilities. *Acta Metall*. 1989;37:1227-1240.
67. Bae IJ, Baik S. Abnormal grain growth of alumina. *J Am Ceram Soc*. 1997;80:1149-1156.
68. Hwang NM. Simulation of the effect of anisotropic grain boundary mobility and energy on abnormal grain growth. *J Mater Sci*. 1998;33:5625-5629.
69. Dillon SJ, Harmer MP, Rohrer GS. The relative energies of normally and abnormally growing grain boundaries in alumina displaying different complexions. *J Am Ceram Soc*. 2010;93:1796-1802.
70. Rheinheimer W, Hoffmann MJ. Non-arrhenius behavior of grain growth in strontium titanate: new evidence for a structural transition of grain boundaries. *Scripta Mater*. 2015;101: 68-71.
71. Sternlicht H, Rheinheimer W, Hoffmann MJ, et al. The mechanism of grain boundary motion in $SrTiO_3$. *J Mater Sci*. 2016;51: 467-475.
72. Burke JE. Lucalox alumina: the ceramic that revolutionized outdoor lighting. *MRS Bulletin*. 1996;21:61-68.
73. Rhodes WH. Controlled transient solid second phase sintering of yttria. *J Am Ceram Soc*. 1981;64:13-19.
74. Greskovich CD, Minnear WP, O'clair CR, Gurmen EO, Riedner RJ. Transparent polycrystalline garnets. U.S. Patent 5,484,750. 1996.
75. Kaysser WA, Petzow G. Liquid phase sintering of ceramics. In: Davis RF, Ill HP, Porter RL, eds. *Chapter 17 in Emergent Process Methods for High-Technology Ceramics*. New York, NY: Plenum Press;1984:225-231.

76. Hampshire S. Silicon nitride ceramics–review of structure, processing and properties. *J Achiev Mater Manuf Eng*. 2007;24:43-50.
77. German RM. *Liquid Phase Sintering*. New York, NY: Springer Science & Business Media; 2013.
78. Marion JE, Hsueh CH, Evans AG. Liquid-phase sintering of ceramics. *J Am Ceram Soc*. 1987;70:708-713.
79. Kwon OH, Messing GL. A theoretical analysis of solution-precipitation controlled densification during liquid phase sintering. *Acta Metall Mater*. 1991;39:2059-2068.
80. Svoboda J, Riedel H, Gaebel R. A model for liquid phase sintering. *Acta Mater*. 1996;44:3215-3226.
81. Mortensen A. Kinetics of densification by solution-reprecipitation. *Acta Mater*. 1997;45:749-758.
82. Kang SJL, Kim KH, Yoon DN. Densification and shrinkage during liquidphase sintering. *J Am Ceram Soc*. 1991;74:425-427.
83. Shaw TM. Model for the effect of powder packing on the driving force for liquid-phase sintering. *J Am Ceram Soc*. 1993;76:664-670.
84. Lee SM, Kang SJL. Theoretical analysis of liquid-phase sintering: pore filling theory. *Acta Mater*. 1998;46:3191-3202.
85. Lee SM, Chaix JM, Martin CL, et al. Computer simulation of particle rearrangement in the presence of liquid. *Inter J Met Mater*. 1999;5:197-203.
86. Parikh NM, Humenik M. Cermets: II, wettability and microstructure studies in liquid-phase sintering. *J Am Ceram Soc*. 1957;40:315-320.
87. Kwon OH, Messing GL. Kinetic analysis of solution-precipitation during liquid-phase sintering of alumina. *J Am Ceram Soc*. 1990;73:275-281.
88. Yang JF, Ohji T, Niihara K. Influence of yttria–alumina content on sintering behavior and microstructure of silicon nitride ceramics. *J Am Ceram Soc*. 2000;83:2094-2096.
89. Kochawattana S, Stevenson A, Lee SH, et al. Sintering and grain growth in SiO_2 doped Nd: YAG. *J Eur Ceram Soc*. 2008;28:1527-1534.
90. Kwon OJ, Yoon DN. Closure of isolated pores in liquid-phase sintering of W-Ni. *Int J Powder Metall Powder Tech*. 1981;17:127-133.
91. Kang SJL, Kaysser WA, Petzow G, et al. Elimination of pores during liquid phase sintering of Mo—Ni. *Powder Metall*. 1984;27:97-100.
92. Park JK, Kang SJL, Eun KY, et al. Microstructural change during liquid phase sintering of W− Ni− Fe alloy. *Metall Trans A*. 1989;20:837-845.
93. Shaw TM. Liquid redistribution during liquid-phase sintering. *J Am Ceram Soc*. 1986;69:27-34.
94. Park HH, Kwon OJ, Yoon DN. The critical grain size for liquid flow into pores during liquid phase sintering. *Metall Trans A*. 1986;17:1915-1919.
95. Kim YP, Jung SW, Kang SJL, et al. Enhanced densification of liquid-phase-sintered WC–Co by use of coarse WC powder: experimental support for the pore-filling theory. *J Am Ceram Soc*. 2005;88:2106-2109.
96. Yang DY, Yoon DY, Kang SJL. Abnormal grain growth enhanced densification of liquid phase-sintered WC–Co in support of the pore filling theory. *J Mater Sci*. 2012;47:7056-7063.
97. Lee SM, Kang SJL. Evaluation of densification mechanisms of liquid-phase sintering. *Z Metallkde*. 2001;92:669-674.
98. Lifshitz IM, Slyozov VV. The kinetics of precipitation from supersaturated solid solutions. *J Phys Chem Solids*. 1961;19:35-50.
99. Wagner C. Theory of precipitate change by redissolution. *Z Elektrochem*. 1961;65:581-591.
100. Ardell AJ. The effect of volume fraction on particle coarsening: theoretical considerations. *Acta Metall*. 1972;20:61-71.
101. German RM, Olevsky EA. Modeling grain growth dependence on the liquid content in liquid-phase-sintered materials. *Metall Mater Trans A*. 1998;29:3057-3067.
102. Kim SG. Large-scale three-dimensional simulation of ostwald ripening. *Acta Mater*. 2007;55:6513-6525.
103. Lee SM, Kang SJL. Microstructure development during liquid-phase sintering. *Z Metallkde*. 2005;96:141-147.
104. Luo J, Wang H, Chiang YM. Origin of solid-state activated sintering in Bi_2O_3-doped ZnO. *J Am Ceram Soc*. 1999;82:916-920.
105. Ackler HD, Chiang YM. Effect of initial microstructure on final intergranular phase distribution in liquid-phase-sintered ceramics. *J Am Ceram Soc*. 1999;82:183-189.
106. Luo J. Liquid-like interface complexion: from activated sintering to grain boundary diagrams. *Curr Opin Solid State Mater Sci*. 2008;12:81-88.
107. Dillon SJ, Harmer MP, Luo J. Grain boundary complexions in ceramics and metals: an overview. *JOM J Min Met Mater Soc*. 2009;61:38-44.
108. Luo J. Developing interfacial phase diagrams for applications in activated sintering and beyond: current status and future directions. *J Am Ceram Soc*. 2012;95:2358-2371.
109. Howe JM. Crystal growth from the liquid. in *Interfaces in Materials: Atomic Structure, Thermodynamics and Kinetics of Solid-Vapor, Solid-Liquid and Solid-Solid Interfaces*. New York, NY: John Wiley & Sons, Inc.;1997:256-268.
110. Jo W, Kim DY, Hwang NM. Effect of interface structure on the microstructural evolution of ceramics. *J Am Ceram Soc*. 2006;89:2369-2380.
111. Kang SJL, Jung YI, Jung SH, et al. Interface structure-dependent grain growth behavior in polycrystals. In: Molodov DA, eds. *Chapter 12 in Microstructural Design of Advanced Engineering Materials*. Weinheim: Wiley-VCH Verlag GmbH & Co.; 2013:299-322.
112. Jung YI, Kang SJL, Yoon DY. Coarsening of polyhedral grains in a liquid matrix. *J Mater Res*. 2009;24:2949-2959.
113. Kang SJL, Han SM. Grain growth in Si_3N_4-based materials. *MRS Bull*. 1995;20:33-37.
114. Park YJ, Hwang NM, Yoon DY. Abnormal growth of faceted (WC) grains in a (Co) liquid matrix. *Metall Mater Trans A*. 1996;27:2809-2819.
115. Oh KS, Jun JY, Kim DY, et al. Shape dependence of the coarsening behavior of niobium carbide grains dispersed in a liquid iron matrix. *J Am Ceram Soc*. 2000;83:3117-3120.
116. Park CW, Yoon DY. Abnormal grain growth in alumina with anorthite liquid and the effect of MgO addition. *J Am Ceram Soc*. 2002;85:1585-1593.
117. Jang CW, Kim J, Kang SJL. Effect of sintering atmosphere on grain shape and grain growth in liquid-phase-sintered silicon carbide. *J Am Ceram Soc*. 2002;85:1281-1284.
118. Choi K, Hwang NM, Kim DY. Effect of grain shape on abnormal grain growth in liquid-phase-sintered $Nb_{1-x}Ti_xC$–Co alloys. *J Am Ceram Soc*. 2002;85:2313-2318.

119. Chung SY, Yoon DY, Kang SJL. Effects of donor concentration and oxygen partial pressure on interface morphology and grain growth behavior in $SrTiO_3$. *Acta Mater*. 2002;50:3361-3371.
120. Yoon BK, Lee BA, Kang SJL. Growth behavior of rounded (Ti, W)C and faceted WC grains in a Co matrix during liquid phase sintering. *Acta Mater*. 2005;53:4677-4685.
121. Heo YH, Jeon SC, Fisher JG, et al. Effect of step free energy on delayed abnormal grain growth in a liquid phase-sintered $BaTiO_3$ model system. *J Eur Ceram Soc*. 2011;31:755-762.
122. Moon KS, Rout D, Lee HY, et al. Effect of TiO_2 addition on grain shape and grain coarsening behavior in $95Na_{1/2}Bi_{1/2}TiO_3$–$5BaTiO_3$. *J Eur Ceram Soc*. 2011;31:1915-1920.
123. Scherer GW. Sintering of low-density glasses: I, theory. *J Am Ceram Soc*. 1977;60:236-239.
124. Mackenzie JK, Shuttleworth R. A phenomenological theory of sintering. *Proc Phys Soc Sec B*. 1949;62:833-852.
125. Scherer GW. Viscous sintering of a bimodal pore-size distribution. *J Am Ceram Soc*. 1984;67:709-715.
126. Scherer GW, Bachman DL. Sintering of low-density glasses: II, experimental study. *J Am Ceram Soc*. 1977;60:239-243.
127. Sacks MD, Tseng TY. Preparation of SiO_2 glass from model powder compacts: I, formation and characterization of powders, suspensions, and green compacts. *J Am Ceram Soc*. 1984;67:526-532.
128. Rabinovich EM. Preparation of glass by sintering. *J Mater Sci*. 1985;20:4259-4297.
129. Scherer GW. Sintering inhomogeneous glasses: application to optical waveguides. *J Non-Cryst Solids*. 1979;34:239-256.
130. Tummala RR. Ceramics in microelectronics packaging: past, present and future. In: Jaccodine R, Jackson KA, Lillie ED, Sundahl RC, eds. *Proceedings of the 4th International Symposium on Electronics Packaging Materials Science*. Cambridge: The Materials Research Society; 1998:379-86.
131. Skorokhod VV. *Rheological Basis of Theory of Sintering*. Kiev: Naukova dumka; 1972.
132. Bordia RK, Scherer GW. On constrained sintering—I. constitutive model for a sintering body. *Acta Metall*. 1988;36:2393-2397.
133. Bordia RK, Scherer GW. On constrained sintering—II. comparison of constitutive models. *Acta Metall*. 1988;36:2399-2409.
134. Bordia RK, Scherer GW. On constrained sintering—III. rigid inclusions. *Acta Metall*. 1988;36:2411-2416.
135. Olevsky EA. Theory of sintering: from discrete to continuum. *Mater Sci Eng R Rep*. 1998;23:41-100.
136. Olevsky EA, Tikare V, Garino T. Multi-scale study of sintering: a review. *J Am Ceram Soc*. 2006;89:1914-1922.
137. Green DJ, Guillon O, Rödel J. Constrained sintering: a delicate balance of scales. *J Eur Ceram Soc*. 2008;28:1451-1466.
138. Skorokhod VV, Olevskii E, Shtern MB. Continuum theory of sintering. I. phenomenological model. analysis of the effect of external forces on the kinetics of sintering. *Powder Metall Met Ceram*. 1993;32:21-26.
139. Skorokhod VV, Olevskii E, Shtern MB. Continuum theory of sintering. II. Effect of the rheological properties of the solid phase on the kinetics of sintering. *Powder Metall Met Ceram*. 1993;32:112-117.
140. Olevsky E, Skorohod V. Some questions of sintering kinetics under external forces influence. Proceedings of Technological and Construction Plasticity of Porous Materials. National Academy of Sciences, IPMS, UA:1988:97-103.
141. Reid CR. Numerical simulation of free shrinkage using a continuum theory for sintering. *Powder Tech*. 1994;81:287-291.
142. Kraft T, Riedel H, Stingl P, et al. Finite element simulation of die pressing and sintering. *Adv Eng Mater*. 1999;1:107-109.
143. Olevsky EA, German RM, Upadhyaya A. Effect of gravity on dimensional change during sintering—II. Shape distortion. *Acta Mater*. 2000;48:1167-1180.
144. Reiterer M, Kraft T, Janosovits U, et al. Finite element simulation of cold isostatic pressing and sintering of SiC components. *Ceram Inter*. 2004;30:177-183.
145. Kraft T, Riedel H. Numerical simulation of solid state sintering; model and application. *J Eur Ceram Soc*. 2004;24:345-361.
146. Ch'ng HN, Pan J. Modelling microstructural evolution of porous polycrystalline materials and a numerical study of anisotropic sintering. *J Comput Phys*. 2005;204:430-461.
147. Reiterer MW, Ewsuk KG, Argüello JG. An arrhenius-type viscosity function to model sintering using the Skorohod-Olevsky viscous sintering model within a finite-element code. *J Am Ceram Soc*. 2006;89:1930-1935.
148. Camacho-Montes H, García-Casillas PE, Rodríguez-Ramos R, et al. Simulation of the stress-assisted densification behavior of a powder compact: effect of constitutive laws. *J Am Ceram Soc*. 2008;91:836-845.
149. Raj R. Analysis of the sintering pressure. *J Am Ceram Soc*. 1987;70:C210-211.
150. Wakai F, Shinoda Y, Akatsu T. Methods to calculate sintering stress of porous materials in equilibrium. *Acta Mater*. 2004;52:5621-5631.
151. Scherer GW. Viscous sintering under a uniaxial load. *J Am Ceram Soc*. 1986;69:C206-207.
152. Scherer GW. Cell models for viscous sintering. *J Am Ceram Soc*. 1991;74:1523-1531.
153. Raj R, Bordia RK. Sintering behavior of bi-modal powder compacts. *Acta Metall*. 1984;32:1003-1019.
154. Jagota A, Dawson PR. Modeling of sintering and traction induced compaction of powders. *J Metals*. 1987;39:A18.
155. Jagota A, Mikeska KR, Bordia RK. Isotropic constitutive model for sintering particle packings. *J Am Ceram Soc*. 1990;73:2266-2273.
156. Du ZZ, Cocks ACF. Constitutive models for the sintering of ceramic components—I. material models. *Acta Metall Mater*. 1992;40:1969-1979.
157. McMeeking RM, Kuhn L. A diffusional creep law for powder compacts. *Acta Metall Mater*. 1992;40:961-969.
158. Riedel H, Zipse H, Svoboda J. Equilibrium pore surfaces, sintering stresses and constitutive equations for the intermediate and late stages of sintering—II. diffusional densification and creep. *Acta Metall Mater*. 1994;42:445-452.
159. Cocks ACF. Constitutive modelling of powder compaction and sintering. *Prog Mater Sci*. 2001;46:201-229.
160. Kim HG, Gillia O, Bouvard D. A phenomenological constitutive model for the sintering of alumina powder. *J Eur Ceram Soc*. 2003;23:1675-1685.
161. Maximenko AL, Olevsky EA. Effective diffusion coefficients in solid-state sintering. *Acta Mater*. 2004;52:2953-2963.
162. Bordia RK, Raj R. Sintering of TiO_2–Al_2O_3 composites: a model experimental investigation. *J Am Ceram Soc*. 1988;71:302-310.

163. Chu MY, De Jonghe LC, Rahaman MN. Effect of temperature on the densification/creep viscosity during sintering. *Acta Metall*. 1989;37:1415-1420.
164. Ducamp VC, Raj R. Shear and densification of glass powder compacts. *J Am Ceram Soc*. 1989;72:798-804.
165. Aulbach E, Zuo R, Rödel J. Laser-assisted high-resolution loading dilatometer and applications. *Exp Mech*. 2004;44:71-75.
166. Venkatachari KR, Raj R. Shear deformation and densification of powder compacts. *J Am Ceram Soc*. 1986;69:499-506.
167. Mikeska KR, Scherer GW, Bordia RK. Constitutive parameters of sintering materials. *Ceram Trans*. 1990;7:200-214.
168. Zuo R, Aulbach E, Bordia RK, et al. Critical evaluation of hot forging experiments: case study in alumina. *J Am Ceram Soc*. 2003;86:1099-1105.
169. Zuo R, Aulbach E, Rödel J. Experimental determination of sintering stresses and sintering viscosities. *Acta Mater*. 2003;51: 4563-4574.
170. Cai PZ, Messing GL, Green DJ. Determination of the mechanical response of sintering compacts by cyclic loading dilatometry. *J Am Ceram Soc*. 1997;80:445-452.
171. Zuo R, Aulbach E, Rödel J. Viscous Poisson's coefficient determined by discontinuous hot forging. *J Mater Res*. 2003;18: 2170-2176.
172. Chang J, Guillon O, Rödel J, et al. Uniaxial viscosity of gadolinium-doped ceria determined by discontinuous sinter forging. *J Eur Ceram Soc*. 2007;27:3127-3133.
173. Lange FF. Processing-related fracture origins: I, observations in sintered and isostatically hot-pressed $A1_2O_3/ZrO_2$ composites. *J Am Ceram Soc*. 1983;66:396-398.
174. Lange FF, Davis BA, Aksay IA. Processing-related fracture origins: III, differential sintering of ZrO_2 agglomerates in Al_2O_3/ZrO_2 composite. *J Am Ceram Soc*. 1983;66:407-408.
175. Becher TN, Becher PF. Sintered Al_2O_3-SiC-whisker composites. *Am Ceram Soc Bull*. 1987;66:339-342.
176. Rahaman MN, De Jonghe LC. Effect of rigid inclusions on the sintering of glass powder compacts. *J Am Ceram Soc*. 1987;70: C348-351.
177. Wu JM, Yeh TS. Sintering of hydroxylapatite-zirconia composite materials. *J Mater Sci*. 1988;23:3771-3777.
178. Boccaccini AR. Sintering of glass matrix composites containing Al_2O_3 platelet inclusions. *J Mater Sci*. 1994;29:4273-4278.
179. Eberstein M, Reinsch S, Müller R, et al. Sintering of glass matrix composites with small rigid inclusions. *J Eur Ceram Soc*. 2009;29:2469-2479.
180. Yan Z, Martin CL, Guillon O, et al. Effect of size and homogeneity of rigid inclusions on the sintering of composites. *Scripta Mater*. 2013;69:327-330.
181. Salamone SM. Densification of and constitutive laws for ceramic matrix composites and multilayered systems; Ph. D Thesis. Seattle, WA:University of Washington; 2003.
182. Hsueh CH, Evans AG, Cannon RM, et al. Viscoelastic stresses and sintering damage in heterogeneous powder compacts. *Acta Metall*. 1986;34:927-936.
183. Scherer GW. Sintering with rigid inclusions. *J Am Ceram Soc*. 1987;70:719-725.
184. Bordia RK, Raj R. Analysis of sintering of a composite with a glass or ceramic matrix. *J Am Ceram Soc*. 1986;69:C55-57.
185. Salamone SM, Stearns LC, Bordia RK, et al. Effect of rigid inclusions on the densification and constitutive parameters of liquid-phase-sintered $YBa_2Cu_3O_{6+x}$ powder compacts. *J Am Ceram Soc*. 2003;86:883-892.
186. Tummala RR. Ceramic and glass-ceramic packaging in the 1990s. *J Am Ceram Soc*. 1991;74:895-908.
187. Imanaka Y. *Multilayered Low Temperature Cofired Ceramics (LTCC) Technology*. New York, NY: Springer Science & Business Media; 2005.
188. Dorey RA, Rocks SA, Dauchy F, et al. Integrating functional ceramics into microsystems. *J Eur Ceram Soc*. 2008;28:1397-1403.
189. Singhal SC. Solid oxide fuel cells: status, challenges and opportunities. *Ind Ceram*. 2008;28:53-59.
190. Stern KH. *Metallurgical and Ceramic Protective Coatings*. London: Chapman and Hall; 1996:194-235.
191. Guillon O, Bordia RK, Martin CL. Sintering of thin films/constrained sintering. In: Fang ZZ, eds. *Chapter 16 in Sintering of Advanced Materials*. Cambridge, UK: Woodhead Publishing Ltd; 2010:414-433.
192. Scherer GW, Garino TG. Viscous sintering on a rigid substrate. *J Am Ceram Soc*. 1985;68:216-220.
193. Bordia RK, Raj R. Sintering behavior of ceramic films constrained by a rigid substrate. *J Am Ceram Soc*. 1985;68:287-292.
194. Hsueh CH. Sintering of a ceramic film on a rigid substrate. *Scripta Metall*. 1985;19:1213-1217.
195. Guillon O, Aulbach E, Rödel J, et al. Constrained sintering of alumina thin films: comparison between experiment and modeling. *J Am Ceram Soc*. 2007;90:1733-1737.
196. Guillon O, Krauß S, Rödel J. Influence of thickness on the constrained sintering of alumina films. *J Eur Ceram Soc*. 2007;27:2623-2627.
197. Stech M, Reynders P, Rödel J. Constrained film sintering of nanocrystalline TiO_2. *J Am Ceram Soc*. 2000;83:1889-1896.
198. Mücke R, Menzler N, Buchkremer HP, et al. Cofiring of thin zirconia films during SOFC manufacturing. *J Am Ceram Soc*. 2009;92:S95-102.
199. Bang J, Lu GQ. Densification kinetics of glass films constrained on rigid substrates. *J Mater Res*. 1995;10:1321-1326.
200. Mohanram A, Lee SH, Messing GL, et al. Constrained sintering of low-temperature co-fired ceramics. *J Am Ceram Soc*. 2006;89:1923-1929.
201. Ollagnier JB, Green DJ, Guillon O, et al. Constrained sintering of a glass ceramic composite: II. symmetric laminate. *J Am Ceram Soc*. 2009;92:2900-2906.
202. Ollagnier JB, Guillon O, Rödel J. Constrained sintering of a glass ceramic composite: I. asymmetric laminate. *J Am Ceram Soc*. 2010;93:74-81.
203. Guillon O, Weiler L, Rödel J. Anisotropic microstructural development during the constrained sintering of dip-coated alumina thin films. *J Am Ceram Soc*. 2007;90:1394-1400.
204. Martin CL, Bordia RK. The effect of a substrate on the sintering of constrained films. *Acta Mater*. 2009;57:549-558.
205. Martin CL, Bordia RK. The effect of a substrate on the microstructure of particulate films. In: Olevsky EA, Bordia RK, eds. *Vol. 209 in Advances in Sintering Science and Technology: Ceramic Transactions*. Hoboken, NJ: John Wiley & Sons, Inc.; 2010:125-133.
206. Bordia RK, Jagota A. Crack growth and damage in constrained sintering films. *J Am Ceram Soc*. 1993;76:2475-2485.

207. Cai PZ, Green DJ, Messing GL. Constrained densification of alumina/zirconia hybrid laminates, I: experimental observations of processing defects. *J Am Ceram Soc*. 1997;80:1929-1939.
208. Tzeng SY, Jean JH. Stress development during constrained sintering of alumina/glass/alumina sandwich structure. *J Am Ceram Soc*. 2002;85:335-340.
209. Martin CL, Camacho-Montes H, Olmos L, et al. Evolution of defects during sintering: discrete element simulations. *J Am Ceram Soc*. 2009;92:1435-1441.
210. Lu GQ, Sutterlin RC, Gupta TK. Effect of mismatched sintering kinetics on camber in a low-temperature cofired ceramic package. *J Am Ceram Soc*. 1993;76:1907-1914.
211. Cai PZ, Green DJ, Messing GL. Constrained densification of alumina/zirconia hybrid laminates, II: viscoelastic stress computation. *J Am Ceram Soc*. 1997;80:1940-1948.
212. Jean JH, Chang CR, Chen ZC. Effect of densification mismatch on camber development during cofiring of nickel-based multilayer ceramic capacitors. *J Am Ceram Soc*. 1997;80:2401-2406.
213. Mohanram A, Messing GL, Green DJ, et al. Prediction of shrinkage and deformation during LTCC device production. *Proc Int Microelectron Packag Soc*. 2002;4931:772-777.
214. Huang R, Pan J. A further report on finite element analysis of sintering deformation using densification data—error estimation and constrained sintering. *J Eur Ceram Soc*. 2008;28:1931-1939.
215. Olevsky E, Molla TT, Frandsen HL, et al. Sintering of multilayered porous structures: part I-constitutive models. *J Am Ceram Soc*. 2013;96:2657-2665.
216. Ni DW, Olevsky E, Esposito V, et al. Sintering of multilayered porous structures: part II–experiments and model applications. *J Am Ceram Soc*. 2013;96:2666-2673.
217. Wilkinson DS, Ashby MF. Pressure sintering by power law creep. *Acta Metall*. 1975;23:1277-1285.
218. Helle AS, Easterling KE, Ashby MF. Hot-isostatic pressing diagrams: new developments. *Acta Metall*. 1985;33:2163-2174.
219. Castañeda PP, Willis JR. On the overall properties of nonlinearly viscous composites. *Proc R Soc Lond Math Phys Eng Sci*. 1988;416:217-244.
220. Besson J, Abouaf M. Rheology of porous alumina and simulation of hot isostatic pressing. *J Am Ceram Soc*. 1992;75:2165-2172.
221. Sofronis P, McMeeking RM. Creep of power-law material containing spherical voids. *J Appl Mech*. 1992;1:S88-95.
222. Olevsky E, Dudek HJ, Kaysser WA. HIPing conditions for processing of metal matrix composites using continuum theory for sintering I. theoretical analysis. *Acta Metall Mater*. 1996;44:707-713.
223. Geindreau C, Bouvard D, Doremus P. Constitutive behaviour of metal powder during hot forming.: part II: unified viscoplastic modelling. *Eur J Mech-A Solids*. 1999;18:597-615.
224. Olevsky EA, Molinari A. Kinetics and stability in compressive and tensile loading of porous bodies. *Mech Mater*. 2006;38:340-366.
225. Song Y, Li YY, Zhou ZY, et al. A multi-field coupled FEM model for one-step-forming process of spark plasma sintering considering local densification of powder material. *J Mater Sci*. 2011;46:5645-5656.
226. Olevsky EA, Garcia-Cardona C, Bradbury WL, et al. Fundamental aspects of spark plasma sintering: II. finite element analysis of scalability. *J Am Ceram Soc*. 2012;95:2414-2422.
227. Rahaman MN, De Jonghe LC. Sintering of spherical glass powder under a uniaxial stress. *J Am Ceram Soc*. 1990;73:707-712.
228. Guillon O, Cao S, Chang J, et al. Effect of uniaxial load on the sintering behaviour of 45S5 bioglass® powder compacts. *J Eur Ceram Soc*. 2011;31:999-1007.
229. Bordia RK, Zuo R, Guillon O, et al. Anisotropic constitutive laws for sintering bodies. *Acta Mater*. 2006;54:111-118.
230. Shang H, Mohanram A, Olevsky E, et al. Evolution of anisotropy in hierarchical porous ceramics during sinter-forging. *J Eur Ceram Soc*. 2016;36:2937-2945.
231. Wonisch A, Guillon O, Kraft T, et al. Stress-induced anisotropy of sintering alumina: discrete element modelling and experiments. *Acta Mater*. 2007;55:5187-5199.
232. Olevsky EA, Kushnarev B, Maximenko A, et al. Modelling of anisotropic sintering in crystalline ceramics. *Phil Mag*. 2005;85:2123-2146.
233. Wakai F, Shinoda Y. Anisotropic sintering stress for sintering of particles arranged in orthotropic symmetry. *Acta Mater*. 2009;57:3955-3964.
234. Wakai F, Bordia RK. Microstructural evolution and anisotropic shrinkage in constrained sintering and sinter forging. *J Am Ceram Soc*. 2012;95:2389-2397.
235. Kim CH, Kim HK. Trend of material development for high-capacitance multi-layer ceramic capacitor. *Ceramist*. 2016;19:62-67.
236. High Growth Potential of MLCC Market for Car Industry. Shinyoung Research Company. Seoul, 2015.
237. Fedorchenko IM, Burenkov GL, Raichenko AI, et al. Electrodischarge reaction sintering of powder mixtures. *Dokl Akad Nauk SSSR*. 1977;236:585-588.
238. Nishimura T, Mitomo M, Hirotsuru H, et al. Fabrication of silicon nitride nano-ceramics by spark plasma sintering. *J Mater Sci Lett*. 1995;14:1046-1047.
239. Munir ZA, Anselmi-Tamburini U, Ohyanagi M. The effect of electric field and pressure on the synthesis and consolidation of materials: a review of the spark plasma sintering method. *J Mater Sci*. 2006;41:763-777.
240. Garay JE. Current-activated, pressure-assisted densification of materials. *Ann Rev Mater Res*. 2010;40:445-468.
241. Olevsky E, Aleksandrova E, Ilyina A, et al. Outside mainstream electronic databases: review of studies conducted in the USSR and post-Soviet countries on electric current-assisted consolidation of powder materials. *Mater*. 2013;6:4375-4440.
242. Grasso S, Sakka Y, Maizza G. Electric current activated/assisted sintering (ECAS): a review of patents 1906–2008. *Sci Tech Adv Mater*. 2009;10:053001.
243. Lee G, Yurlova MS, Giuntini D, et al. Densification of zirconium nitride by spark plasma sintering and high voltage electric discharge consolidation: a comparative analysis. *Cer Int*. 2015;41:14973-14987.
244. Liu L, Ye F, Zhou Y, et al. Fast bonding α-SiAlON ceramics by spark plasma sintering. *J Eur Ceram Soc*. 2010;30:2683-2689.
245. Pinc WR, Di Prima M, Walker LS, et al. Spark plasma joining of ZrB_2–SiC composites using zirconium–boron reactive filler layers. *J Am Ceram Soc*. 2011;94:3825-3832.
246. Rizzo S, Grasso S, Salvo M, et al. Joining of C/SiC composites by spark plasma sintering technique. *J Eur Ceram Soc*. 2014;34:903-913.

247. Groza J. Field activation provides improved sintering. *Met Powder Rep*. 2000;7:16-18.
248. Olevsky E, Froyen L. Constitutive modeling of spark-plasma sintering of conductive materials. *Scripta Mater*. 2006;55:1175-1178.
249. Olevsky E, Kandukuri S, Froyen L. Consolidation enhancement in spark-plasma sintering: impact of high heating rates. *J Appl Phys*. 2007;102:114913.
250. Olevsky E, Kandukuri S, Froyen L. Analysis of mechanisms of spark-plasma sintering. *Key Eng Mater*. 2008;368–72:1580-1584.
251. Olevsky E, Froyen L. Influence of thermal diffusion on spark-plasma sintering. *J Am Ceram Soc*. 2009;92:S122-132.
252. Garcia C, Olevsky E. Numerical simulation of spark plasma sintering. *Adv Sci Tech*. 2010;63:58-61.
253. Olevsky EA, Bradbury WL, Haines CD, et al. Fundamental aspects of spark plasma sintering: I. experimental analysis of scalability. *J Am Ceram Soc*. 2012;95:2406-2413.
254. Zavaliangos A, Zhang J, Krammer M, et al. Temperature evolution during field activated sintering. *Mater Sci Eng, A*. 2004; 379:218-228.
255. Anselmi-Tamburini U, Gennari S, Garay JE, et al. Fundamental investigations on the spark plasma sintering/synthesis process: II. modeling of current and temperature distributions. *Mater Sci Eng, A*. 2005;394:139-148.
256. Vanmeensel K, Laptev A, Hennicke J, et al. Modelling of the temperature distribution during field assisted sintering. *Acta Mater*. 2005;53:4379-4388.
257. Wang X, Casolco SR, Xu G, et al. Finite element modeling of electric current-activated sintering: the effect of coupled electrical potential, temperature and stress. *Acta Mater*. 2007;55:3611-3622.
258. Grasso S, Sakka Y, Maizza G. Pressure effects on temperature distribution during spark plasma sintering with graphite sample. *Mater Trans*. 2009;50:2111-2114.
259. Wang C, Cheng LF, Zhao Z. FEM analysis of the temperature and stress distribution in spark plasma sintering: modelling and experimental validation. *Comp Mater Sci*. 2010;49:351-362.
260. Munoz S, Anselmi-Tamburini U. Temperature and stress fields evolution during spark plasma sintering processes. *J Mater Sci*. 2010;45:6528-6539.
261. Wei X, Giuntini D, Maximenko AL, et al. Electric contact resistance in spark plasma sintering tooling setup. *J Am Ceram Soc*. 2015;98:3553-60.
262. Giuntini D, Raethel J, Herrmann M, et al. Spark plasma sintering novel tooling design: temperature uniformization during consolidation of silicon nitride powder. *J Ceram Soc Jpn*. 2016;124:403-414.
263. Giuntini D, Raethel J, Herrmann M, et al. Advancement of tooling for spark plasma sintering. *J Am Ceram Soc*. 2015;98:3529-3537.
264. Vanmeensel K, Laptev A, Van der Biest O, et al. The influence of percolation during pulsed electric current sintering of ZrO_2–TiN powder compacts with varying TiN content. *Acta Mater*. 2007;55:1801-1811.
265. Maizza G, Grasso S, Sakka Y. Moving finite-element mesh model for aiding spark plasma sintering in current control mode of pure ultrafine WC powder. *J Mater Sci*. 2009;44:1219-1236.
266. McWilliams B, Zavaliangos A, Cho KC, et al. The modeling of electric-current-assisted sintering to produce bulk nanocrystalline tungsten. *JOM*. 2006;58:67-71.
267. McWilliams B, Zavaliangos A. Multi-phenomena simulation of electric field assisted sintering. *J Mater Sci*. 2008;43:5031-5035.
268. Zhang J, Zavaliangos A. Discrete finite-element simulation of thermoelectric phenomena in spark plasma sintering. *J Electron Mater*. 2011;40:873-878.
269. Giuntini D, Olevsky EA, Garcia-Cardona C, et al. Localized overheating phenomena and optimization of spark-plasma sintering tooling design. *Materials*. 2013;6:2612-2632.
270. Li W, Olevsky EA, McKittrick J, et al. Densification mechanisms of spark plasma sintering: multi-step pressure dilatometry. *J Mater Sci*. 2012;47:7036-7046.
271. Aleksandrova EV, Ilyina AM, Grigoryev EG, et al. Contribution of electric current into densification kinetics during spark plasma sintering of conductive powder. *J Am Ceram Soc*. 2015;98:3509-3517.
272. Langer J, Hoffmann MJ, Guillon O. Direct comparison between hot pressing and electric field-assisted sintering of submicron alumina. *Acta Mater*. 2009;57:5454-5465.
273. Langer J, Hoffmann MJ, Guillon O. Electric field-assisted sintering in comparison with the hot pressing of yttria-stabilized zirconia. *J Am Ceram Soc*. 2011;94:24-31.
274. Langer J, Hoffmann MJ, Guillon O. Electric field-assisted sintering and hot pressing of semiconductive zinc oxide: a comparative study. *J Am Ceram Soc*. 2011;94:2344-2353.
275. Katz JD. Microwave sintering of ceramics. *Annu Rev Mater Sci*. 1992;22:153-170.
276. Agawal DK. Microwave processing of ceramics: a review. *Curr Opin Solid State Mater Sci*. 1998;3:480-486.
277. Cheng J, Agrawal D, Zhang Y, et al. Fabricating transparent ceramics by microwave sintering: focus on electronics. *Am Ceram Soc Bull*. 2000;79:71-74.
278. Brosnan KH, Messing GL, Agrawal DK. Microwave sintering of alumina at 2.45 GHz. *J Am Ceram Soc*. 2003;86:1307-1312.
279. Willert-Porada M, A microstructural approach to the origin of "microwave effects" in sintering of ceramics and composites. In: Clark DE, Sutton WH, Lewis DA, eds. *Vol. 80 in Microwaves: Theory and Application in Materials Processing IV*. Westerville, OH: American Ceramic Society, 1997:153-163.
280. Rybakov KI, Olevsky EA, Semenov VE. The microwave ponderomotive effect on ceramic sintering. *Scripta Mater*. 2012; 66:1049-1052.
281. Rybakov KI, Olevsky EA, Krikun EV. Microwave sintering: fundamentals and modeling. *J Am Ceram Soc*. 2013;96:1003-1020.
282. Olevsky EA, Maximenko AL, Grigoryev EG. Ponderomotive effects during contact formation in microwave sintering. *Modelling Simul Mater Sci Eng*. 2013;21:055022.
283. Birnboim A, Carmel Y. Simulation of microwave sintering of ceramic bodies with complex geometry. *J Am Ceram Soc*. 1999;82:3024-3030.
284. Riedel H, Svoboda J. Simulation of microwave sintering with advanced sintering models.In: Willert-Porada M, eds. *Chapter 23 in Advances in Microwave and Radio Frequency Processing*. New York, NY: Springer Science & Business Media; 2006:210-216.
285. Bouvard D, Charmond S, Carry CP. Finite element modeling of microwave sintering. In: Olevsky EA, Bordia RK, eds. *Vol. 209 in Advances in Sintering Science and Technology*. Hoboken, NJ: Ceramic Ceram. Transactions, 2010:173-180.

286. Manière C, Zahrah T, Olevsky EA. Inherent heating instability of direct microwave sintering process: sample analysis for porous 3Y-ZrO_2. *Scripta Mater*. 2017;128:49-52.
287. Manière C, Zahrah T, Olevsky EA. Fully coupled electromagnetic-thermal-mechanical comparative simulation of direct vs. hybrid microwave sintering of 3Y-ZrO2. *J Am Ceram Soc*. 2017; http://onlinelibrary.wiley.com/doi/10.1111/jace.14762/full.
288. Cologna M, Rashkova B, Raj R. Flash sintering of nanograin zirconia in< 5 s at 850°C. *J Am Ceram Soc*. 2010;93:3556-3559.
289. Cologna M, Prette ALG, Raj R. Flash-sintering of cubic yttria-stabilized zirconia at 750°C for possible use in SOFC manufacturing. *J Am Ceram Soc*. 2011;94:316-319.
290. Prette ALG, Cologna M, Sglavo V, et al. Flash-sintering of Co_2MnO_4 spinel for solid oxide fuel cell applications. *J Power Sources*. 2011;196:2061-2065.
291. Cologna M, Francis JSC, Raj R. Field assisted and flash sintering of alumina and its relationship to conductivity and MgO-doping. *J Eur Ceram Soc*. 2011;31:2827-2837.
292. Hao X, Liu Y, Wang Z, et al. A novel sintering method to obtain fully dense gadolinia doped ceria by applying a direct current. *J Power Sources*. 2012;210:86-91.
293. Yoshida H, Sakka Y, Yamamoto T, et al. Densification behaviour and microstructural development in undoped yttria prepared by flash-sintering. *J Eur Ceram Soc*. 2014;34:991-1000.
294. Raj R. Joule heating during flash-sintering. *J Eur Ceram Soc*. 2012;32:2293-2301.
295. Baraki R, Schwarz S, Guillon O. Effect of electrical field/current on sintering of fully stabilized zirconia. *J Am Ceram Soc*. 2012;95:75-78.
296. Park J, Chen IW. In situ thermometry measuring temperature flashes exceeding 1700°C in 8 mol% Y_2O_3-stablized zirconia under constant-voltage heating. *J Am Ceram Soc*. 2013;96:697-700.
297. Dong Y, Chen IW. Onset criterion for flash sintering. *J Am Ceram Soc*. 2015;98:3624-3627.
298. Olevsky EA, Rolfing SM, Maximenko AL. Flash(ultra-rapid) spark-plasma sintering of silicon carbide. *Nat Sci Rep*. 2016;6:33408.
299. Harmer MP, Brook RJ. Fast firing-microstructural benefits. *Trans J Br Ceram Soc*. 1981;80:147-148.
300. Kim DH, Kim CH. Effect of heating rate on pore shrinkage in yttria-doped zirconia. *J Am Ceram Soc*. 1993;76:1877-1878.
301. Johnson DL. Ultra-rapid sintering. *Mater Sci Res*. 1984;16:243-252.
302. Chu MY, De Jonghe LC, De Jonghe MKF, et al. Precoarsening to improve microstructure and sintering of powder compacts. *J Am Ceram Soc*. 1991;74:2902-2911.
303. Lin FJT, De Jonghe LC, Rahaman MN. Microstructure refinement of sintered alumina by a two-step sintering technique. *J Am Ceram Soc*. 1997;80:2269-2277.
304. Chen IW, Wang XH. Sintering dense nanocrystalline ceramics without final-stage grain growth. *Nature*. 2000;404:168-171.
305. Wang XH, Deng XY, Bai HL, et al. Two-step sintering of ceramics with constant grain-size, II: $BaTiO_3$ and Ni–Cu–Zn ferrite. *J Am Ceram Soc*. 2006;89:438-443.
306. Bodišová K, Šajgalík P, Galusek D, et al. Two-stage sintering of alumina with submicrometer grain size. *J Am Ceram Soc*. 2007;90:330-332.
307. Ko SY, Kang SJL. Growth behavior of faceted $Na_{1/2}Bi_{1/2}TiO_3$-$BaTiO_3$ grains in single and two-step sintering. *J Eur Ceram Soc*. 2016;36:1159-1165.
308. Duran P, Capel F, Tartaj J, et al. A strategic two-stage low-temperature thermal processing leading to fully dense and fine-grained doped-ZnO varistors. *Adv Mater*. 2002;14:137-141.
309. Lee YI, Kim YW, Mitomo M, et al. Fabrication of dense nanostructured silicon carbide ceramics through two-step sintering. *J Am Ceram Soc*. 2003;86:1803-1805.
310. Kim HD, Park YJ, Han BD, et al. Fabrication of dense bulk nano-Si_3N_4 ceramics without secondary crystalline phase. *Scripta Mater*. 2006;54:615-619.
311. Yang DY, Yoon DY, Kang SJL. Suppression of abnormal grain growth in WC–Co via two-step liquid phase sintering. *J Am Ceram Soc*. 2011;94:1019-1024.
312. Chen PL, Chen IW. Sintering of fine oxide powders: II, sintering mechanisms. *J Am Ceram Soc*. 1997;80:637-645.
313. Coble RL. Sintering alumina: effect of atmospheres. *J Am Ceram Soc*. 1962;45:123-127.
314. Kang SJL, Yoon KJ. Densification of ceramics containing entrapped gases. *J Eur Ceram Soc*. 1989;5:135-139.
315. Yan MF. Microstructural control in the processing of electronic ceramics. *Mater Sci Eng*. 1981;48:53-72.
316. Readey DW, Lee J, Quadir T Vapor transport and sintering of ceramics. In: Kuczynski GC, Miller AE, Sargent GA, eds. *Chapter 9 in Materials Science Research*. New York, NY: Plenum Press;1984:115-136.
317. Readey MJ, Readey DW. Sintering of ZrO_2 in HCl atmospheres. *J Am Ceram Soc*. 1986;69:580-582.
318. Dole SL, Prochazka S, Doremus RH. Microstructural coarsening during sintering of boron carbide. *J Am Ceram Soc*. 1989;72:958-966.
319. German RM. Coarsening in sintering: grain shape distribution, grain size distribution, and grain growth kinetics in solid-pore systems. *Crit Rev Solid State Mater Sci*. 2010;35:263-305.
320. Yamasaki N, Yanagisawa K, Nishioka M, et al. A hydrothermal hot-pressing method: apparatus and application. *J Mater Sci Lett*. 1986;5:355-356.
321. Sōmiya S. Hydrothermal preparation and sintering of fine ceramic powders. In: Sōmiya S, eds. *Chapter 9 in Hydrothermal Reactions for Materials Science and Engineering*. New York, NY: Springer Science & Business Media; 1989:46-62.
322. DeSilva P, Bucea L, Sirivivatnanon V, et al. Carbonate binders by "cold sintering" of calcium carbonate. *J Mater Sci*. 2007;42:6792-6797.
323. Guo J, Guo H, Baker AL, et al. Cold sintering: a paradigm shift for processing and integration of ceramics. *Angew Chem*. 2016;128(38):11629-11633.
324. Guo H, Baker A, Guo J, et al. Cold sintering process: a novel technique for low-temperature ceramic processing of ferroelectrics. *J Am Ceram Soc*. 2016;99:3489-3507.
325. Guo H, Baker A, Guo J, et al. Protocol for ultralow-temperature ceramic sintering: an integration of nanotechnology and the cold sintering process. *ACS Nano*. 2016;10:10606-10614.
326. Guo H, Guo J, Baker A, et al. Hydrothermal-assisted cold sintering process: a new guidance for low-temperature ceramic sintering. *ACS Appl Mater Interfaces*. 2016;8:20909-20915.
327. Pan J. *Computer modelling of sintering at different length scales*. London: Springer-Verlag, London; 2017.

328. Maximenko A, Kuzmov A, Grigoryev E, et al. Modeling sintering without constitutive equations. *Am Ceram Soc Bull*. 2012;91:14-15.
329. Maximenko A, Kuzmov A, Grigoryev E, et al. Direct multiscale modeling of sintering. *J Am Ceram Soc*. 2012;95:2383-2388.
330. Bordère S. Original Monte Carlo methodology devoted to the study of sintering processes. *J Am Ceram Soc*. 2002;85:1845-1852.
331. Bordère S, Gendron D, Bernard D. Improvement in the accuracy of calculated interface morphologies within Monte Carlo simulations of sintering processes. *Scripta Mater*. 2006;55:267-270.
332. DeHoff RT. Stereological theory of sintering. In: Uskoković P, Ill HP, Spriggs RM, eds. *Chapter 3 in Science of Sintering*. New York, NY: Springer US; 1989:55-71.
333. Bouvard D, McMeeking RM. Deformation of interparticle necks by diffusion-controlled creep. *J Am Ceram Soc*. 1996;79:666-672.
334. Svoboda J, Riedel H, Zipse H. Equilibrium pore surfaces, sintering stresses and constitutive equations for the intermediate and late stages of sintering—I. computation of equilibrium surfaces. *Acta Metall Mater*. 1994;42:435-443.
335. Tsuruta K, Omeltchenko A, Kalia RK, et al. Early stages of sintering of silicon nitride nanoclusters: a molecular-dynamics study on parallel machines. *Europhysics Lett*. 1996;33:441-446.
336. Huilong Z, Averback RS. Sintering of nano-particle powders: simulations and experiments. *Mater Manuf Process*. 1996;11:905-923.
337. Zeng P, Zajac S, Clapp PC, et al. Nanoparticle sintering simulations. *Mater Sci Eng, A*. 1998;252:301-306.
338. Vashishta P, Bachlechner ME, Campbell T, et al. Multimillion atom simulations of nanostructured materials on parallel computers sintering and consolidation, fracture, and oxidation. *Progr Theor Phys Supp*. 2000;138:175-190.
339. Koparde VN, Cummings PT. Molecular dynamics simulation of titanium dioxide nanoparticle sintering. *J Phys Chem B*. 2005;109:24280-24287.
340. Zhang W, Schneibel JH. The sintering of two particles by surface and grain boundary diffusion—a two-dimensional numerical study. *Acta Metall Mater*. 1995;43:4377-4386.
341. Zhou H, Derby JJ. Three-dimensional finite-element analysis of viscous sintering. *J Am Ceram Soc*. 1998;81:533-540.
342. Cannon RM, Carter WC. Interplay of sintering microstructures, driving forces, and mass transport mechanisms. *J Am Ceram Soc*. 1989;72:1550-1555.
343. Wakai F, Katsura K, Kanchika S, et al. Sintering force behind the viscous sintering of two particles. *Acta Mater*. 2016;109:292-299.
344. Wakai F. Modeling and simulation of elementary processes in ideal sintering. *J Am Ceram Soc*. 2006;89:1471-1484.
345. Wakai F, Gómez-Garcia D, Domínguez-Rodríguez A. Pore channel closure in sintering of a ring of three spheres. *J Eur Ceram Soc*. 2007;27:3365-3370.
346. Wakai F, Akatsu T. Anisotropic viscosities and shrinkage rates in sintering of particles arranged in a simple orthorhombic structure. *Acta Mater*. 2010;58:1921-1929.
347. Martin CL, Schneider LCR, Olmos L, et al. Discrete element modeling of metallic powder sintering. *Scripta Mater*. 2006;55:425-428.
348. Henrich B, Wonisch A, Kraft T, et al. Simulations of the influence of rearrangement during sintering. *Acta Mater*. 2007;55:753-762.
349. Martin CL, Yan Z, Jauffres D, et al. Sintered ceramics with controlled microstructures: numerical investigations with the discrete element method. *J Ceram Soc Jpn*. 2016;124:340-345.
350. Jauffrès D, Martin CL, Lichtner A, et al. Simulation of the elastic properties of porous ceramics with realistic microstructure. *Model Simul Mater Sci Eng*. 2012;20:045009.
351. Jauffres D, Martin CL, Lichtner A, et al. Simulation of the toughness of partially sintered ceramics with realistic microstructures. *Acta Mater*. 2012;60:4685-4694.
352. Roussel D, Lichtner A, Jauffrès D, et al. Strength of hierarchically porous ceramics: discrete simulations on X-ray nanotomography images. *Scripta Mater*. 2016;113:250-253.
353. Roussel D, Lichtner A, Jauffrès D, et al. Effective transport properties of 3D multi-component microstructures with interface resistance. *Comp Mater Sci*. 2015;96:277-283.
354. Hassold GN, Chen IW, Srolovitz DJ. Computer simulation of final-stage sintering: I, model kinetics, and microstructure. *J Am Ceram Soc*. 1990;73:2857-2864.
355. Tikare V, Braginsky M, Olevsky EA. Numerical simulation of solid-state sintering: I, sintering of three particles. *J Am Ceram Soc*. 2003;86:49-53.
356. Tikare V, Braginsky M, Olevsky E, et al. Numerical simulation of anisotropic shrinkage in a 2D compact of elongated particles. *J Am Ceram Soc*. 2005;88:59-65.
357. Braginsky M, Tikare V, Olevsky E. Numerical simulation of solid state sintering. *Int J Solids Struct*. 2005;42:621-636.
358. Dynys FW, Halloran JW. Influence of aggregates on sintering. *J Am Ceram Soc*. 1984;67:596-601.
359. Pan J. Solid-state diffusion under a large driving force and the sintering of nanosized particles. *Phil Mag Lett*. 2004;84:303-310.
360. Giuntini D, Olevsky EA. Sintering stress of nonlinear viscous materials. *J Am Ceram Soc*. 2016;99:3520-3524.
361. Wong KV, Hernandez A. A review of additive manufacturing. *ISRN Mech Eng*. 2012;73:1-12.
362. Conner BP, Manogharan GP, Martof AN, et al. Making sense of 3-D printing: creating a map of additive manufacturing products and services. *Addit Manuf*. 2014;1:64-76.
363. Fischer P, Romano V, Weber HP, et al. Sintering of commercially pure titanium powder with a Nd: YAG laser source. *Acta Mater*. 2003;51:1651-1662.
364. Gu DD, Meiners W, Wissenbach K, et al. Laser additive manufacturing of metallic components: materials, processes and mechanisms. *Int Mater Rev*. 2012;57:133-164.
365. Onagoruwa S, Bose S, Bandyopadhyay A. Fused deposition of ceramics (FDC) and composites. Proceedings of the 12th International Solid Freeform Fabrication(SFF) Symposium. Ausin, TX; 2001:224-31.
366. Bertrand P, Bayle F, Combe C, et al. Ceramic components manufacturing by selective laser sintering. *Appl Surf Sci*. 2007;254:989-992.
367. Wilkes J, Hagedorn YC, Meiners W, et al. Additive manufacturing of ZrO_2-Al_2O_3 ceramic components by selective laser melting. *Rapid Prototyp J*. 2013;19:51-57.
368. Travitzky N, Bonet A, Dermeik B, et al. Additive manufacturing of ceramic-based materials. *Adv Eng Mater*. 2014;16:729-754.

369. Maximenko A, Van der Biest O, Olevsky E. Modeling of damage development during sintering of ceramics. *Int J Fracture*. 2001;110:9-14.
370. Olevsky EA, Shoales GA, German RM. Temperature effect on strength evolution under sintering. *Mater Res Bull*. 2001;36:449-459.
371. Olevsky E, Maximenko A, Ivlev Y. Shape distortion under isostatic pressing. *J Mater Sci Lett*. 1997;16:1270-1273.
372. Olevsky EA, Wang X, Maximenko A, et al. Fabrication of net-shape functionally graded composites by electrophoretic deposition and sintering: modeling and experimentation. *J Am Ceram Soc*. 2007;90:3047-3056.
373. Onoda GY, Hench LL. *Ceramic Processing Before Firing*. New York, NY: John Wiley; 1978.
374. Smith JP, Messing GL. Sintering of bimodally distributed alumina powders. *J Am Ceram Soc*. 1984;67:238-242.
375. Parfitt GD, Peacock J. *Surface and Colloid Science (Vol. 10)*. New York, NY: Plenum press;1978.

How to cite this article: Bordia RK, Kang S-JL, Olevsky EA. Current understanding and future research directions at the onset of the next century of sintering science and technology. *Journal of the American Ceramic Society*, 2017;100:2314-2352. https://doi.org/.10.1111/jace.14919

AUTHOR BIOGRAPHIES

Rajendra K. Bordia is a Professor and Chair of the Materials Science and Engineering Department at Clemson University in Clemson, SC, USA. He was a faculty member at the University of Washington (1991–2013) and a Research Scientist in DuPont Co. (1986–1991). He received his B.Tech from IIT, Kanpur, India (1979), and his M.S. (1981) and Ph.D. (1986) from Cornell University, Ithaca, NY, USA. His research is at the intersection of materials and mechanics and is currently focused on fundamental and applied studies in the processing and properties of complex material systems for energy, environmental and medical applications. He has authored or co-authored over 130 peer-reviewed technical publications and over 120 technical reports. He was elected Fellow of the American Ceramic Society (2002); Fellow of the Indian Institute of Metals (2010); and an Academician in the World Academy of Ceramics (2012). Other significant awards include: the Humboldt Research award from the Alexander von Humboldt Foundation, Germany (2007); the Marsha Landolt Distinguished Graduate Mentor award from the University of Washington (2007); and the Outstanding Educator Award of the American Ceramic Society (2012). He is an Associate Editor of the Journal of the American Ceramic Society; Editor of the Journal of Ceramic Processing Research; and Editor-in-Chief of the Ceramics International.

Suk-Joong L. Kang is President of the Korea Institute of Ceramic Engineering and Technology (KICET). Before joining KICET in 2015, he was a Professor and a Distinguished Professor in the Department of Materials Science and Engineering at KAIST for 35 years. He received his M.S. from KAIST, Dr.-Ing. from the Ecole Centrale de Paris, and Dr. d'Etat from the University of Paris VI. Prof. Kang is the author of the text *Sintering: Densification, Grain Growth and Microstructure*, published in 2005. He has published more than 280 papers on sintering and microstructural evolution in ceramics and metals. He developed the "Pore Filling Theory" of liquid phase sintering. He suggested the mixed mechanism of boundary migration, and introduced the mixed mechanism principle of microstructural evolution. Prof. Kang is a fellow of the American Ceramic Society, an honorary fellow of the European Ceramic Society, and a member of the World Academy of Ceramics. He served as President of the Korean Ceramic Society and as Editor-in-Chief of the Journal of Asian Ceramic Societies. He is a recipient of the Sosman Award from the American Ceramic Society, the Richard Brook Award from the European Ceramic Society, the Helmholtz International Fellow Award, the Inchon Prize from the Inchon Memorial Foundation, and the Korea Engineering Prize from the President of the Republic of Korea.

Eugene Olevsky is Distinguished Professor of Mechanical Engineering and Associate Dean for Graduate Studies and Research at the College of Engineering of the San Diego State University, USA. Dr. Olevsky is the Director of the San Diego State University Powder Technology Laboratory and also an Adjunct Professor of Nanoengineering at the University of California, San Diego. Prof. Olevsky has obtained two M.S. degrees in Mechanical Engineering and Applied Mathematics and Ph.D. degree in Materials Engineering. Dr. Olevsky's primary area of expertise is in experimentation and computational modeling on powder processing, including novel ceramic, metallic, and composite materials synthesis. Eugene Olevsky is the author of over 500 scientific publications and of more than 150 plenary, keynote, and invited presentations in the area of sintering research. Prof. Olevsky has supervised scientific sintering studies of more than 100 postdoctoral, graduate, and undergraduate students. Dr. Olevsky is an editorial board member of many scientific journals including Powder Metallurgy and Science of Sintering. Prof. Olevsky is a Fellow of the American Ceramic Society, a Fellow of the American Society of Mechanical Engineers, Humboldt Fellow; he is a Full Member of the International Institute of Science of Sintering. Dr. Olevsky's most recent research is focused on field-assisted sintering techniques and sintering-assisted additive manufacturing.